JOURNAL OF CAVE AND KARST STUDIES

March 2025
Volume 87, Number 1
ISSN 1090-6924
A Publication of the National Speleological Society

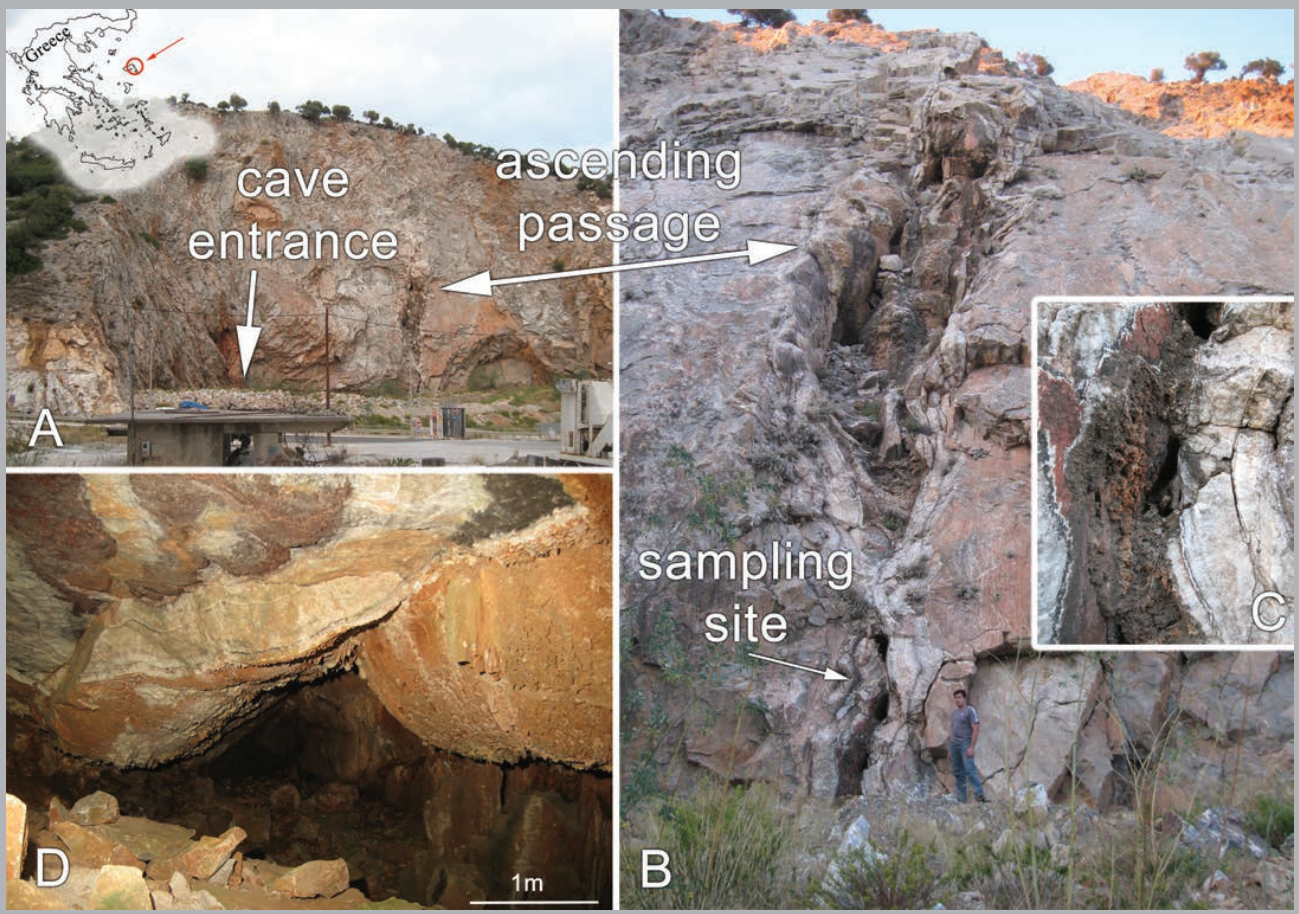

DEDICATED TO THE ADVANCEMENT OF SCIENCE, EDUCATION, EXPLORATION, AND CONSERVATION

Published By
The National Speleological Society

http://caves.org/pub/journal

Office
6001 Pulaski Pike NW
Huntsville, AL 35810 USA
Tel:256-852-1300
nss@caves.org

Editor-in-Chief
Malcolm S. Field
Washington, DC
703-347-8601
field.malcolm1@gmail.com

Production Editor
Scott A. Engel
Knoxville, TN
225-281-3914
saecaver@gmail.com

Copyeditor
Bert Ashbrook
caving.ashbrook@comcast.net

Meredith Hall Weberg
merecaver@yahoo.com

The *Journal of Cave and Karst Studies* , ISSN 1090-6924, CPM Number #40065056, is a multi-disciplinary, refereed journal published four times a year by the National Speleological Society. The *Journal* is available by open access on its website, or check the website for current print subscription rates. Back issues are available from the NSS office.

POSTMASTER: send address changes to the National Speleological Society Office listed above.

The Journal of Cave and Karst Studies is covered by the following ISI Thomson Services Science Citation Index Expanded, ISI Alerting Services, and Current Contents/Physical, Chemical, and Earth Sciences.

Copyright © 2025
by the National Speleological Society, Inc.

BOARD OF EDITORS

Anthropology
George Crothers
University of Kentucky
Lexington, KY
george.crothers@utk.edu

Conservation-Life Sciences
Julian J. Lewis & Salisa L. Lewis
Lewis & Associates, LLC.
Borden, IN
lewisbioconsult@aol.com

Earth Sciences
Benjamin Schwartz
Texas State University
San Marcos, TX
bs37@txstate.edu

Yongli Gao
University of Texas at San Antonio
yongli.gao@utsa.edu

Mario Parise
University Aldo Moro
Bari, Italy
mario.parise@uniba.it

Carol Wicks
Louisiana State University
Baton Rouge, LA
cwicks@lsu.edu

Exploration
Paul Burger
National Park Service
Eagle River, Alaska
paul_burger@nps.gov

Microbiology
Sarah Keenan
South Dakota School of Mines and Technology
Rapid City, SD
Sarah.Keenan@sdsmt.edu

Paleontology
Greg McDonald
National Park Service
Fort Collins, CO
greg_mcdonald@nps.gov

Social Sciences
Joseph C. Douglas
Volunteer State Community College
Gallatin, TN
615-230-3241
joe.douglas@volstate.edu

Book Reviews
Arthur N. Palmer & Margaret V Palmer
State University of New York
Oneonta, NY
palmeran@oneonta.edu

Front Cover: Photographs of unnamed cave on Lesvos Island, Greece. See Lazaridis et al this issue.

Georgios Lazaridis, Lambrini Papadopoulou, Vasilos Melfos, Panagiotis Voudouris. Description of Manganese events in hydrothermal hypogene speleogenesis. *Journal of Cave and Karst Studies*, v. 87, no. 1, p. 1-12. DOI:10.4311/2023ES0102

DESCRIPTION OF MANGANESE EVENTS IN HYDROTHERMAL HYPOGENE SPELEOGENESIS

Georgios Lazaridis,[1,C] Lambrini Papadopoulou,[1] Vasilos Melfos,[1] Panagiotis Voudouris[2]

ABSTRACT

The phreatic speleothems of hydrothermal speleogenesis are mainly mammillaries and spar calcite. In this study, seven samples from four caves in three areas of Greece are investigated. Morphological evidence from these caves along with the presence of the phreatic calcite indicate their hydrothermal origin. The analyzed calcite deposits contain layers of metallic oxides that were investigated with scanning electron microscopy aided by energy dispersive spectrometer semi-quantitative measurements. Their chemical composition is dominated by manganese. Rarely, double-terminated phantom calcite crystals display two repetitions of these manganese oxide layers along the growth surfaces, but most commonly mammillaries exhibit one to four manganese oxide layers. In one case, the manganese layer was formed along with partial dissolution of the calcite that resulted in small pits on the growth surfaces. We interpret these layers in the phantom spar crystals and cave mammillaries to changes in the fluid conditions and fluctuations that are common in phantom crystals result in the deposition of mangese oxides along with or without contemporary dissolution. In order to mark the changes in conditions of their formation, these layers are described as “manganese events.” Because of the low deposition rate of the mammillaries, the repetitions of manganese events are plausibly independent of exogenous factors, such as seeping water. This event can be found in the secondary minerals of both shallow and deep phreatic settings of hydrothermal speleogenesis. The available data set shows that the manganese event is part of a repetitive depositional pattern that appears in at least 17 % of the carbonate speleothems of hydrothermal speleogenesis.

INTRODUCTION

Hypogene speleogenesis driven by carbonic acid can potentially form minerals deposited during a cave’s shift from the dissolutional phase to the depositional phase of speleogenesis. These secondary minerals make up speleothem types such as cave mammillaries and cave spar (Polyak et al., 2008; Polyak et al., 2014, Decker et al., 2018) and are commonly composed of carbonate minerals. In this paper we define cave mammillaries as finely crystalline, often-fibrous, calcite coatings that exhibit a mammillary or botryoidal form on the speleothem surface and likely form in the shallow phreatic zone. We define cave spar as coarsely crystalline, commonly euhedral calcite crystal druses that likely form in the deeper phreatic zone. In some cases, cave spar is characterized by the presence of one or more “phantom” or “ghostly” outlines or shapes within the crystal itself. These outlines appear as faint, often-translucent layers or inclusions that resemble the crystal’s outer shape but are slightly different in color or transparency. Subsequently, these speleothems are informative for at least the latest stages of speleogenesis. Based on these ideas, an extensive study of hypogene caves in Greece has been done to determine conditions during speleogenesis better. During this study, it was noticed that apart from calcite, these cave deposits may contain layers of metallic oxide minerals; i.e., minerals that contain one or more metallic oxide elements. Metallic oxides and hydroxides are one of the main mineral groups that occur in a cave environment, after carbonates and sulfates (Hill and Forti, 1997). They are commonly found as coatings and crusts in both epigene (e.g. Carmichael and Bräuer, 2015; Hill and Forti, 1997; Jones, 1992; Onac et al., 1997) and hypogene caves (e.g. Cunningham et al., 1995; Rossi et al., 2010; Northup et al., 2000; Peck, 1986; Spilde et al., 2005). Furthermore, manganese oxides from caves are often related to microbial activities (Allouc and Harmelin, 2001; Carmichael and Bräuer, 2015; Carmichael et al., 2013a; Carmichael et al., 2013b; Carmichael et al., 2015; Cunningham et al., 1995; Frierdich et al., 2011; Gázquez et al., 2012; Gradziński et al., 1995; Moore, 1981; Northup et al., 2000; Papier et al., 2011; Peck, 1986; Rossi et al., 2010; Spilde et al., 2005).

Mobilization of manganese is controlled by low values of Eh and pH, while increased values lead to deposition in the form of manganese oxides and hydroxides (Hill and Forti, 1997; Onac, 1996). In some cases, they are considered to mark abrupt paleonvironmental changes (Gázquez et al., 2011). Although there are many studies of ferromanganese oxides in caves, their presence, extent, and frequency in hydrothermal calcite deposits is not sufficiently documented. It is worth mentioning that hydrothermal speleogenesis is included in hypogene speleogenesis and consequently when the term “hydrothermal” is used below, it corresponds to hydrothermal hypogene. Moreover, the role of these layers in hypogene speleogenesis remains questionable. This paper documents of their presence in cave mammillaries and cave spar, herein considered hydrothermal speleothems, and discusses their depositional setting.

[1] School of Geology, Aristotle University of Thessaloniki, GR-54124, Thessaloniki, Greece
[2] Faculty of Geology and Geoenvironment, National and Kapodistrian University of Athens, GR-15784, Zografou, Athens, Greece
[C] Corresponding author: geolazarides@gmail.com

SAMPLING AND SPELEOGENESIS

About one hundred hypogene caves in Greece have been identified and systematically researched for deposits that are related to the speleogenetic processes, such as spar and mammillaries (see Lazaridis, 2017, for a brief description of these caves). In total, 24 caves were sampled and among 62 samples manually extracted with a hammer, 7 (locations are seen in Figs. 1–4) were noticed to include distinct metallic oxide layers (Fig. 5). Of these, samples Sp39 and Sp42 come from the mammillaries of the first and second sampling sites in the caves of Lesvos Island, respectively; sample Sp14 is a phantom calcite crystal from Krya Vrysi Cave, and sample Sp16 was collected from Nychteridon Cave at Petralona. In the last, four distinct layers from one mammillary that are referred below as samples Sp16/1 to Sp16/4 were studied.

Lesvos Island

The first sampling site where metallic oxide layers were identified is an unnamed karst cave that was discovered during quarry works and a road construction (Fig. 1A). The lower part of the cave is a horizontal chamber coated with cave mammillaries that connects with a fracture guided ascending channel. Evidence of this vertical channel can also be observed outside the cave in the quarried escarpment. Its height is approximately 12 m and both sidewalls are covered with calcite mammillaries with a thickness of a few tens of centimeters.

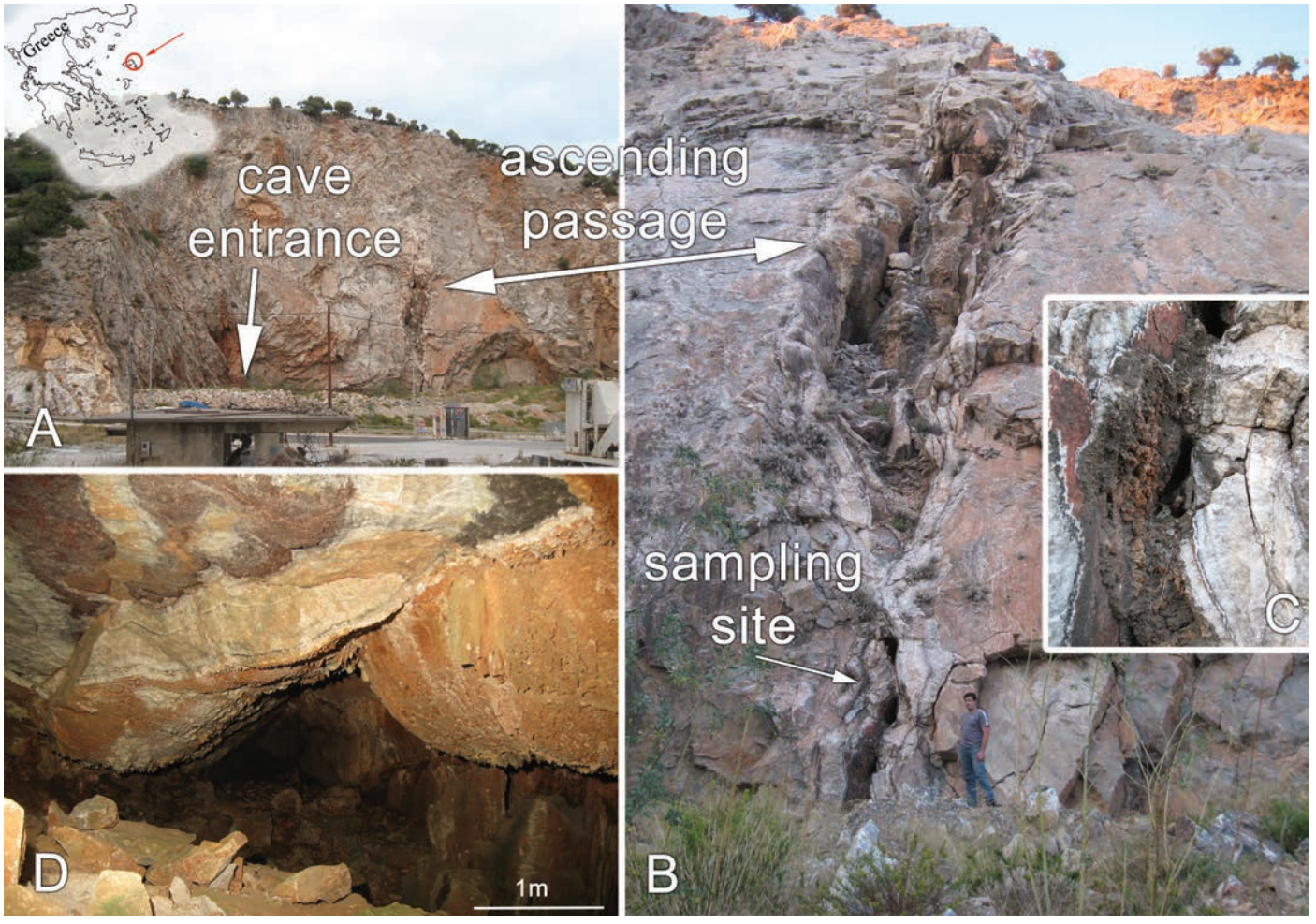

Figure 1. Photographs of unnamed cave (first sampling site) on Lesvos Island, Greece. (*A*) The escarpment where the entrance of the sampled cave and the ascending passage are located. Left white arrow, cave entrance. Right white arrow, ascending passage. Upper left corner inset, map of Greece with the cave location (red circle and arrow). (*B*) Ascending passage (upper white arrow) filled with mammillaries. Lower white arrow, where sample Sp39 was collected. (C) Detail of the sampling site. (D) Similar mammillaries inside the cave, with scale bar.

The second sampling site is located approximately 1.5 km north of the Mytilene port. In this area there are some small unnamed caves that are lined with calcite crystals and mammillaries (Fig. 2). In one case, the sampled mammillaries demonstrate alternations of red and white calcite, with a metallic oxide intercalation between these layers.

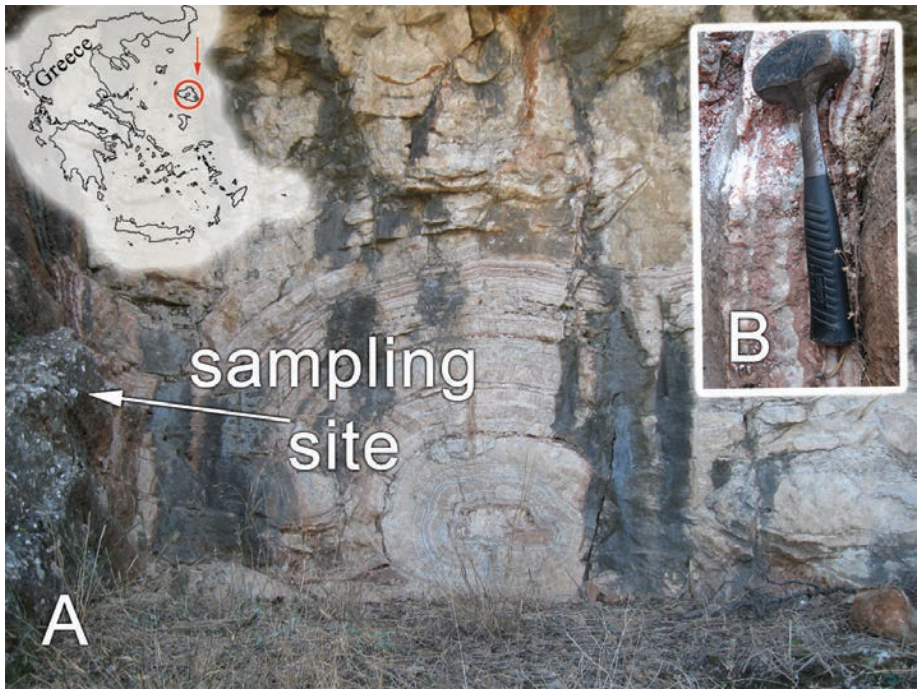

Figure 2. Photographs of unnamed cave (second sampling site) on Lesvos Island. (*A*) Cave filled with mammillary calcite crusts. White arrow, sampling site for sample Sp42. Upper left corner inset, map of Greece with the cave location (red circle and arrow). (*B*) Detail of sample Sp42.

Figure 3. Photograph of Nychteridon Cave with scale bar. Upper left corner inset, map of Greece with the cave location (red circle and arrow). Sample Sp16 sampling site at a natural cross-section of mammillaries. Upper right corner inset, plan view of the cave (based on Oikonomidis et al., 2022) with sampling site (red circle) and scale bar.

Both caves investigated are within the recrystallized limestones of the Pelagonian Zone (Thomaidou, 2009).

Nychteridon Cave, Petralona

Nychteridon Cave (Fig. 3) is located on the Chalkidiki Peninsula, Northern Greece, close to Petralona Cave, which is well-known for an exceptionally preserved skull of *Homo heidelbergensis*. Based on previous studies by Lazaridis (2009) and Veni et al. (2009), the origin of Petralona Cave is attributed to hypogene speleogenesis. Nychteridon Cave is a challenging cave due to bad air conditions in its lower levels. Its morphology is strongly affected by breakdown. In passages located to the periphery of the cave area, where breakdown has not significantly affected the original dissolutional morphology, mammillaries can be observed. The cave displays a hypogene morphological suite, such as maze patterns, cupolas, partitions, blind passages, feeders etc. A 72 cm thick mammillary was sampled, in which four metallic-oxide layers were identified.

Krya Vrysi, Karditsa

The Kyra Vrysi Cave near the village with the same name is located in the vicinity of the city of Karditsa (Fig. 4) and has been only partially explored. It has at least two entrances that were opened due to previous quarry works in a limestone outcrop of the Pindos Zone. Its deeper parts are filled with water. One of its main chambers is lined with doubly terminated scalenohedral calcite crystals. The largest of these crystals can reach about 9 cm in length. They are clear enough to observe metallic oxide coatings along growth surfaces, forming phantom crystals. At least two repetitions of metallic oxide zones have been found in a single crystal.

ANALYTICAL METHODS

Representative samples with metallic oxide layers were morphologically and chemically investigated at the Scanning Microscope Laboratory of the Aristotle University of Thessaloniki, using a JEOL JSM6390 LV scanning electron microscope (SEM) equipped with an INCA 300 energy dispersive spectrometer (EDS) with 20 kV accelerating voltage and 0.4 mA probe current and, for higher magnifications, a FESEM JEOL JSM 7610 FPlus SEM. For SEM observations, the samples were coated with carbon (to an average thickness of 200 × 10^{-10} m) using a JEOL-4X vacuum evaporator. The SEM-EDS semi-quanti-

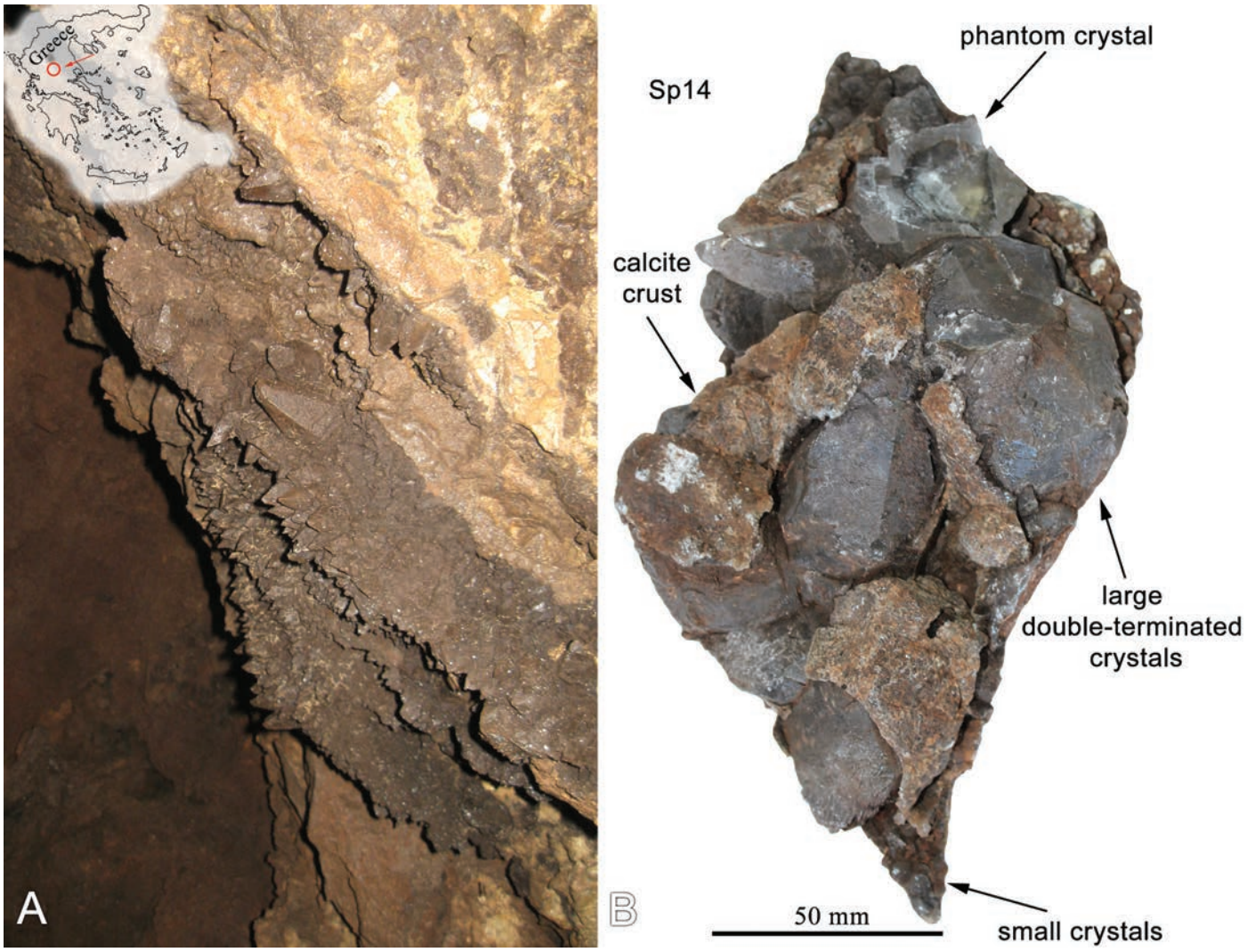

Figure 4. Photographs from Krya Vrysi Cave, in the vicinity of Karditsa, Greece. (A) Calcite spars where sample Sp14 was collected. Upper left corner inset, map of Greece with cave location (red circle and arrow). (B) Sample Sp14 with scale bar, showing an aggregate of large double-terminated calcite crystals, with layers seen as phantom crystals, where metallic oxide layers along growth surfaces can be observed, and small crystals. The sample was originally covered by the calcite *crust* that appears to partially cover the crystals.

tative elemental analysis technique analysis allows the chemical determination of phases with a size as small as 1 × 1 μm. Prior to SEM-EDS, X-ray powder diffraction analyses failed to identify the manganese-bearing minerals.

To access the major and trace element composition of calcite samples, atomic emission spectrometry and inductively coupled plasma mass spectrometry were used, respectively. Microthermometric data from calcite fluid inclusions were obtained using a Linkam THM-600/TMS 90 heating-freezing stage coupled to a Leitz SM-LUX-POL microscope housed at the Department of Mineralogy, Petrology, and Economic Geology of the Aristotle University of Thessaloniki.

RESULTS

Hydrothermal Hypogene Speleogenesis

Cave morphology and geochemistry of secondary minerals have been studied in order to interpret the speleogenesis of the four studied caves. Morphological evidence was based on the presence of maze-cave patterns and some meso- and micro-scale morphological features such as feeders and vertical passages that serve as ascending water input and output points, respectively (Fig. 1B and Fig. 2). Furthermore, the complete hypogene morphological suite, such as the cupolas and related forms, was observed in these caves. Regarding the geochemical evidence, some preliminary data from fluid inclusions indicate mean homogenization temperatures for the Lesvos and Krya Vrysi Caves at 171 °C and 174 °C, respectively. In the Petralona area, where Nychteridon Cave is found, the geothermal field is of lower temperature, 31 °C to 42 °C (Lohnert and Papakonstntinou, 1988; Dotsika et al., 2010). Geochemical evidence from the studied calcite samples relates them to the existing geothermal fields. The presence of greater abundances of trace

elements such as arsenic, zinc, and uranium are indicative of the contribution of geothermal fluids to speleogenesis.

Manganese Layers

The samples from the caves on Lesvos Island (samples Sp39 and Sp42) are similar in their chemical composition. The dominating element is manganese followed by barium, zinc, and iron (Table 1). Sample Sp39 displays higher iron

Table 1. Elemental composition based upon SEM-EDS analysis (columns) in different numbered locations on the magnesium oxide layers from the samples taken from mammillaries in the caves on Lesvos Island (rows). Final row under each sample is the mean value for the sample.

Event and Sample	Mass Percent Element						
	Mass % Ca	Mass % Mn	Mass % Fe	Mass % Zn	Mass % Ba	Mass % O	Mass % S
Sp39-1	bdl	53.56	6.07	bdl	20.64	19.74	bdl
Sp39-2	bdl	57.14	bdl	bdl	23.48	19.38	bdl
Sp39-3	bdl	77.45	bdl	bdl	bdl	22.55	bdl
Sp39-4	2.29	49.63	10.23	5.89	10.95	21.01	bdl
Sp39-5	bdl	58.10	bdl	bdl	22.38	19.53	bdl
Sp39 mean	0.38	59.18	3.26	1.18	15.49	20.44	**bdl**
Sp42-1	bdl	55.04	2.12	2.68	20.48	19.68	bdl
Sp42-2	bdl	56.16	bdl	6.00	17.92	19.91	bdl
Sp42-3	2.36	53.18	2.85	5.65	15.52	20.44	bdl
Sp42-4	2.42	50.04	0.11	3.04	22.19	20.88	1.32
Sp42-5	bdl	58.19	1.01	3.09	17.66	20.05	bdl
Sp42 mean	0.96	54.52	1.22	4.09	18.75	20.19	0.26

Note: bdl indicates below detection limit.

concentration in a few areas. Calcium and sulfur have also been detected in some parts of the metallic oxide layer. The two samples differ mainly in morphology. This can also be detected macroscopically (Figs. 5 and 6), where sample Sp39 demonstrates a relatively high porosity. When observed in the SEM, small cavities are observed to be lined with a layer of manganese oxides with globular shapes (Fig. 6B and C). In some cases, networks of filaments were observed (Fig. 6D). In sample Sp42, only a thin layer of the metallic oxide crust can be seen, well attached to calcite.

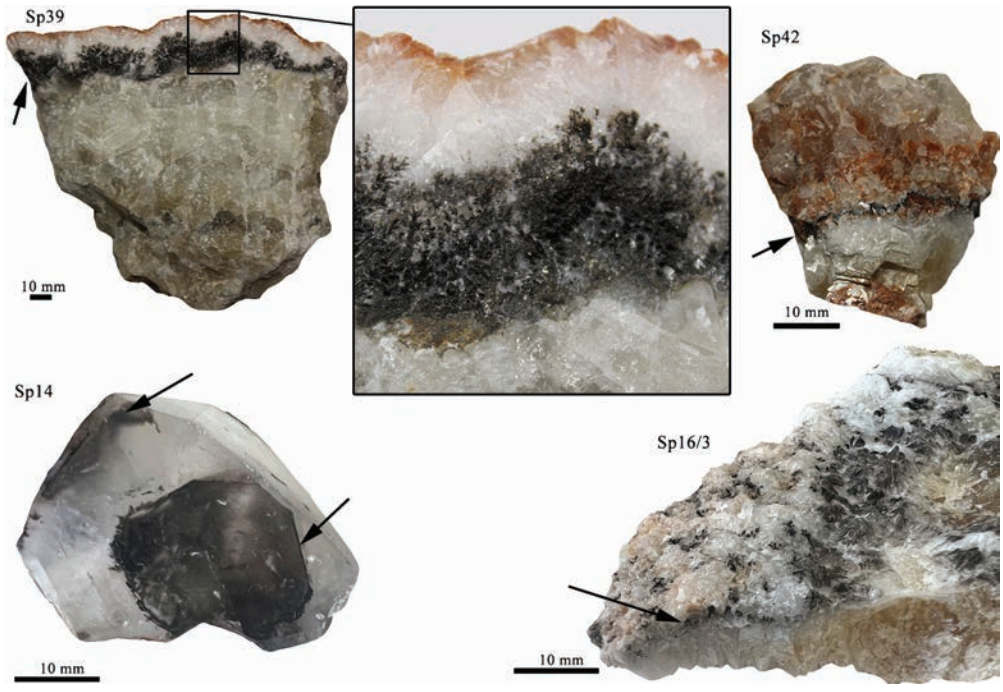

Figure 5. Photographs of representative carbonate deposits of hydrothermal speleogenesis with manganese layers (black arrows), with scale bars. Upper left, sample Sp39 from the mammillaries in the first sampling site of Lesvos Island. Upper center, detail of sample Sp39 displaying the high porosity of the metallic oxide layer. Upper right, sample Sp42 from the mammillaries in the second sampling site of Lesvos Island. Lower left, sample Sp14, a phantom calcite crystal from Krya Vrysi Cave. Lower right, sample Sp16/3, collected from Nychteridon Cave at Petralona.

The metallic oxides from Nychteridon Cave form layers of a few micrometers thick with a few porous areas and a wavy surface. Their chemical composition is dominated by manganese (Table 2). Iron content varies between layers, and higher concentrations were noticed in samples Sp16/1 and Sp16/4. Other elements such as nickel, calcium, magnesium, and silicon have been detected, while barium and aluminum were not found

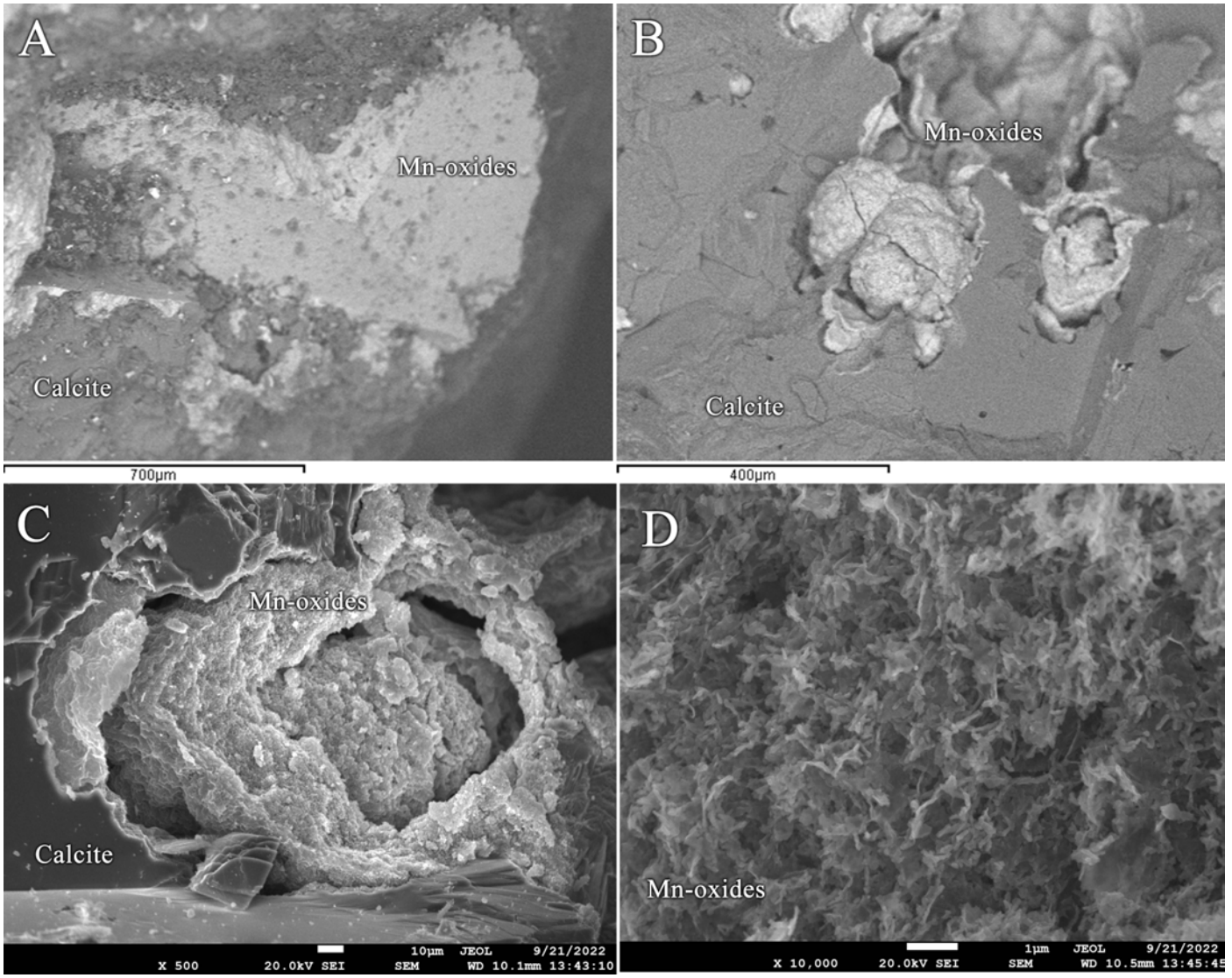

Figure 6. Backscattered SEM images of samples from the Lesvos Island with scale bars below each image. (A) Sample Sp42. (B–C) Sample Sp39. Dissolution cavities in calcite (where indicated) are lined with globular aggregates of manganese oxides (where indicated). (D) Typical networks of manganese oxide filaments forming the globular aggregates.

in all layers. Sample Sp16/3 contains phosphorus and sulfur. In sample Sp16/4, an unidentified mineral composed of cerium (58.90 mass %), calcium (22.16 mass %), and oxygen (18.94 mass %) was observed (Fig. 7).

Sample Sp14 from Krya Vrysi Cave includes a small calcite spar druse (<1 cm) deposited on the bedrock and larger, double-terminated, calcite-spar crystals. All these spars are covered by clastic sediment and by a calcite crust that is a few millimeters in thickness. Macroscopically, dark zones occur along growth surfaces of the crystals. These zones are chemically dominated by manganese. In the SEM this is observed as a thin layer (Fig. 8).

DISCUSSION

The studied metallic oxide layers are incorporated in calcite mammillary and spar coatings that we interpret to have formed under hydrothermal conditions, and their chemical composition is dominated by manganese. Jones (1992) studied the manganese cold water precipitates in various speleothems of the karst terrain at Grand Cayman, such as stalactites, karst breccias, caymanite, terrestrial oncoids, and root calcretes, along fractures and cavities in a dolostone. He found that the manganese oxide precipitation, some of which was stalactitic, had marked distinct stages in the development of the host deposit. In some cases, he also noted repetitions in the paragenetic sequence. The cases studied by Jones (1992), such as the stalactites, are not related to hydrothermal speleogenesis. However, it is worth noting that the manganese oxide precipitates mark changes in the formation process. Similarly, the deposition of hydrothermal calcite is interrupted and replaced by manganese-dominated metallic oxide coatings that mark changes in the formation con-

Table 2. Elemental composition based on SEM-EDS analysis (columns) in different numbered locations on manganese oxide layers from the mammillaries in Nychteridon Cave (rows). Final row under each sample is the mean value for the sample.

Event and Sample	Mass Percent Element										
	Mass % Mg	Mass % Al	Mass % Si	Mass % P	Mass % S	Mass % Ca	Mass % Mn	Mass % Fe	Mass % Ni	Mass % Ba	Mass % O
Sp16/4-1	3.67	6.86	bdl	bdl	bdl	10.40	33.77	13.87	3.89	bdl	27.54
Sp16/4-2	2.20	4.79	bdl	bdl	bdl	7.17	40.74	15.40	3.81	bdl	25.89
Sp16/4-3	1.99	4.98	5.44	bdl	bdl	7.49	30.50	17.64	2.44	bdl	29.53
Sp16/4-4	bdl	3.12	1.41	bdl	bdl	18.47	33.18	15.22	2.23	bdl	26.38
Sp16/4-5	bdl	3.12	1.41	bdl	bdl	18.47	33.18	15.22	2.23	bdl	26.38
Sp16/4-6	2.60	3.77	bdl	bdl	bdl	7.15	44.05	13.11	3.79	bdl	25.53
Sp16/4-7	bdl	3.83	1.77	0.8	0.75	10.33	25.54	28.04	1.40	bdl	27.55
Sp16/4 mean	1.79	4.35	1.79	0.14	0.11	11.35	34.42	16.93	2.83	bdl	26.97
Sp16/3-1	2.05	6.49	0.50	1.29	0.92	7.87	41.17	7.45	3.33	bdl	28.92
Sp16/3-2	bdl	2.28	0.46	1.29	bdl	20.40	35.98	8.59	4.48	bdl	26.52
Sp16/3-3	3.43	6.82	bdl	bdl	0.41	6.52	40.47	9.16	5.69	bdl	27.50
Sp16/3-4	bdl	3.55	bdl	0.77	1.23	7.78	41.77	9.55	4.77	4.72	25.85
Sp16/3-5	3.11	6.84	bdl	bdl	bdl	9.71	37.97	9.74	5.33	bdl	27.30
Sp16/3-6	1.37	3.81	bdl	bdl	bdl	12.06	42.70	6.64	7.83	bdl	25.58
Sp16/3 mean	1.66	4.97	0.16	0.56	0.43	10.72	40.01	8.52	5.24	0.79	26.95
Sp16/2-1	bdl	bdl	bdl	bdl	bdl	10.65	56.70	3.32	2.53	3.93	22.86
Sp16/2-2	bdl	bdl	bdl	bdl	bdl	23.63	44.07	0.78	2.51	5.22	23.78
Sp16/2-3	bdl	bdl	1.63	bdl	bdl	5.19	61.85	bdl	bdl	8.40	22.92
Sp16/2-4	3.85	bdl	bdl	bdl	bdl	12.85	50.50	2.36	2.16	4.17	24.12
Sp16/2-5	3.25	bdl	bdl	bdl	bdl	2.23	60.84	2.27	3.17	5.36	22.88
p16/2 mean	1.42	bdl	0.32	bdl	bdl	10.91	54.79	1.74	1.99	5.42	23.31
Sp16/1-1	3.00	5.20	1.81	bdl	bdl	10.52	31.16	16.92	3.61	bdl	27.77
Sp16/1-2	bdl	4.98	1.65	bdl	bdl	19.07	25.94	18.36	2.56	bdl	27.44
Sp16/1-3	3.09	6.27	bdl	bdl	bdl	13.24	29.83	17.81	2.42	bdl	27.34
Sp16/1-4	3.09	6.27	bdl	bdl	bdl	13.24	29.83	17.81	2.42	bdl	27.34
Sp16/1-5	4.37	6.23	bdl	bdl	bdl	10.90	33.20	14.90	2.89	bdl	27.50
Sp16/1 mean	2.71	5.79	0.69	bdl	bdl	13.39	29.99	17.16	2.78	bdl	27.48

Note: bdl indicates below detection limit.

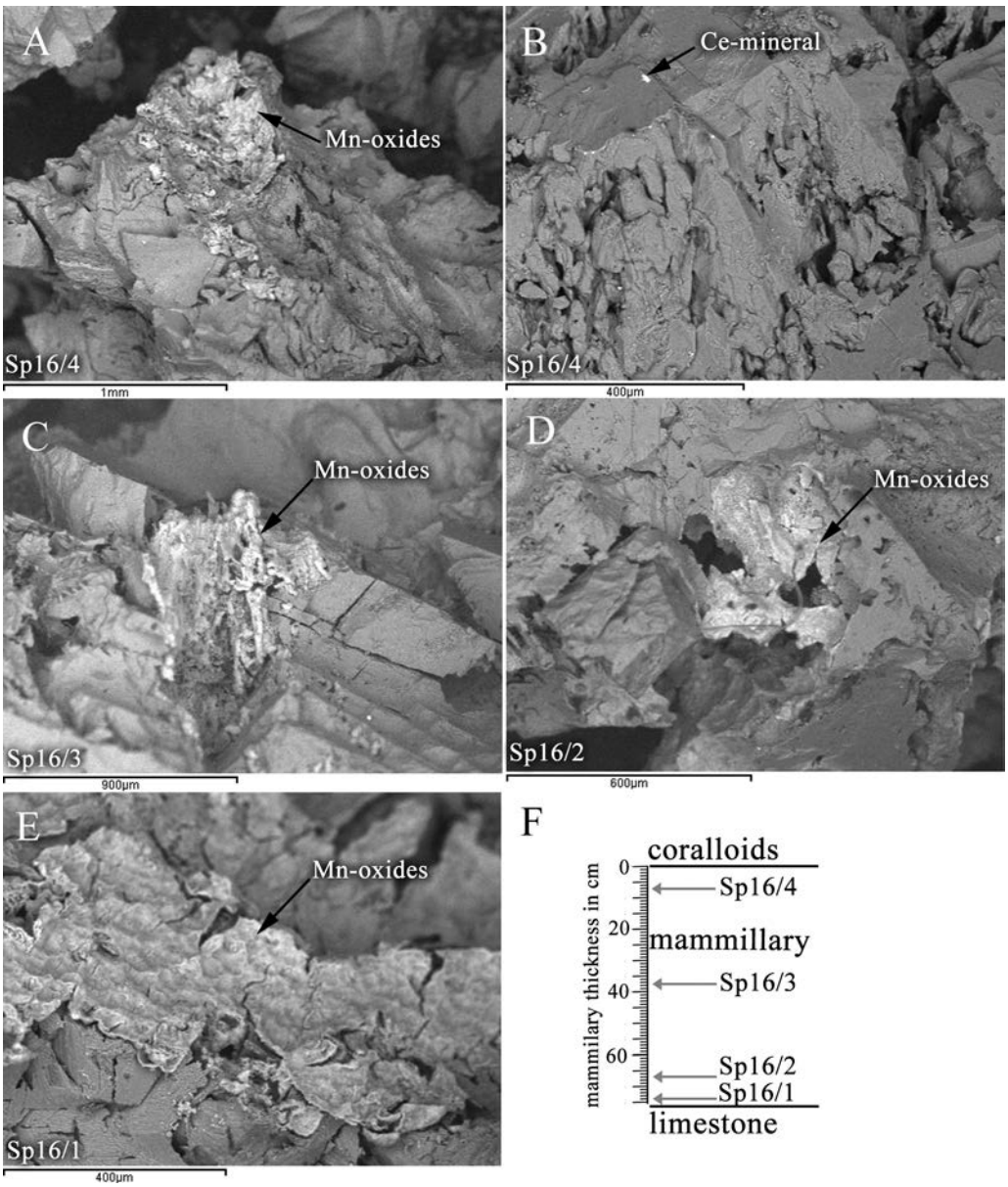

Figure 7. (A–E) SEM images of calcites and layers from samples 16/1–4 taken from a mammillary in Nychteridon Cave. Black arrows show manganese oxide precipitates (A, C–E) and an unidentified cerium mineral (B). Scale bars shown below each image. (F) Chart depicting stratigraphic position of each sample Sp16/1 to Sp16/4 relative to the thickness of the sampled mammillary.

ditions of the sampled speleothems. To mark these changes, hereafter they are called "manganese events."

Frequency and Phreatic Conditions

Based on the systematic sampling and study of Greek hypogene caves, at least 17% of the known hydrothermal caves in Greece contain manganese events that form distinct layers. These layers are suggested to have been formed during interruptions of calcite deposition. In 14 out of 24 sampled caves, the calcite forms cave spar, and the manganese event occurs in one (7 %) of them. Among the 10 caves where the calcite does not form cave spar and where the hydrothermal calcite forms mammillaries, two (20 %) display manganese layers. These two types of hydrothermal deposits, the mammillaries and cave spar, have been considered to be the "byproducts" of hydrothermal speleogenesis in shallow and deep phreatic environments, respectively (Polyak et al., 2008; Polyak et al., 2014). In a cave like Krya Vrysi Cave that only contains cave spar, that fact indicates that the cave formed deeply. Caves with mammillaries, such as those of Lesvos Island and Petralona, experienced shallow conditions conducive to mammillary deposition. Both phreatic environments allow the occurrence of a manganese event, although shallow conditions may be considered more favorable.

Repetitive Character

In the cave spar crystals from Krya Vrysi Cave, the presence of manganese was noticed at the growth surface of phantom crystals. This type of crystal occurs due to fluctuation systems, changes in the chemical composition, pH-Eh, and pressure and temperature conditions of the hydrothermal fluids (Tarassov et al., 2017). As a result, the continuity of crystal growth is interrupted, and dissolution or deposition of other mineral phases occurs. The presence of the two layers of manganese in the studied spar indicates that the manganese event not only indicates changes in the deposition process, but also shows a type of event that could be repeated multiple times during hydrothermal speleogenesis. Considering that the manganese layers in the mammillaries represent similar changes in depositional conditions, it seems that at least four such repetitions occurred.

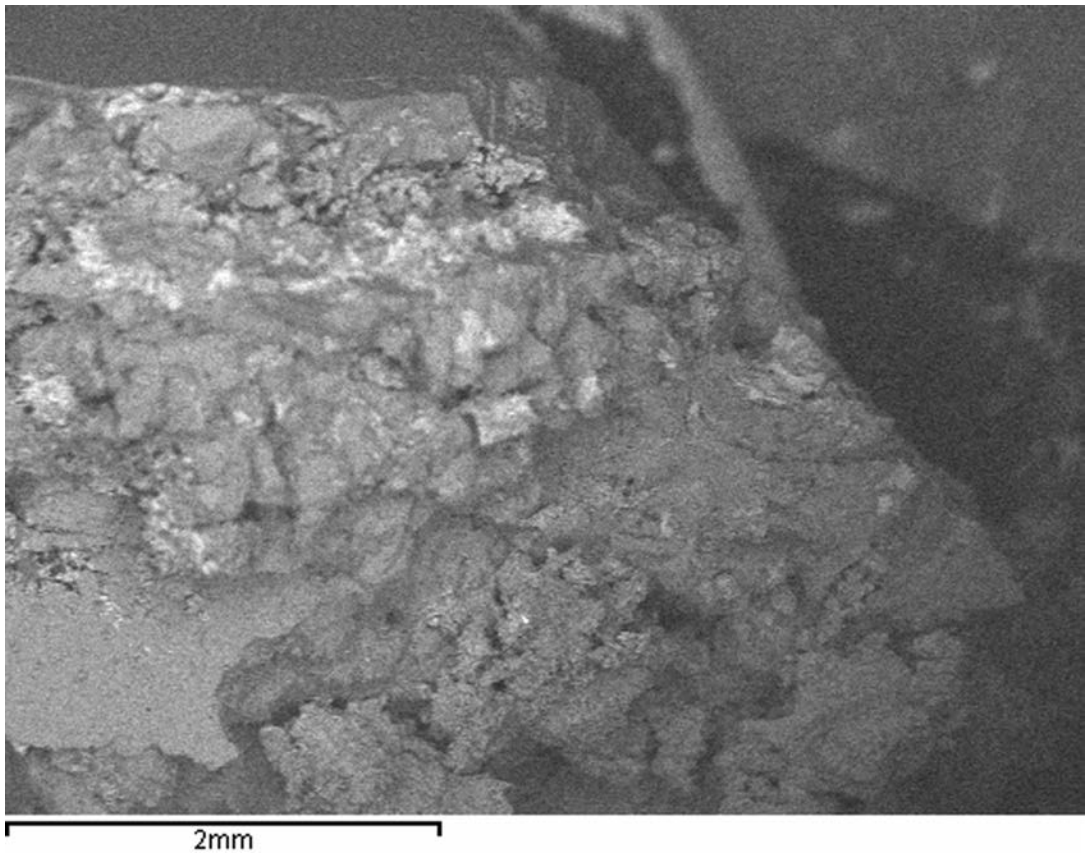

Figure 8. Backscattered SEM image of Sample Sp14 from Krya Vrysi Cave, with scale bar. Dark areas are calcite and bright areas correspond to manganese oxide layer.

Table 3. Elemental composition based on SEM-EDS analysis (columns) in different numbered locations on the manganese oxide layers from the phantom calcite of sample Sp14 from Krya Vrysi Cave (rows).

Event and Sample	Mass Percent Element		
	Mass % Ca	Mass % Mn	Mass % O
Sp14-1	10.14	66.46	23.40
Sp14-2	7.56	69.25	23.19
Sp14-3	11.35	65.14	23.50
Sp14-4	20.75	54.96	24.29
Sp14-5	5.89	71.06	23.05
Sp14-6	34.74	39.80	25.46
Sp14 mean	15.07	61.11	23.81

Note: bdl indicates below detection limit. Final row is the mean value for the sample.

Role of Surface Input

Manganese oxides commonly enter the cave systems by stream or occasionally by dripping water. A question that arises is whether any chemical changes are due to input of meteoric water from adjacent areas above the cave. By definition, hypogene speleogenesis includes only caves where the water comes from lower hydrostratigraphic units and not from downward-flowing water above the cave (Klimchouk, 2017). However, mixing of deep-seated with shallow waters along their rising flow is common in some types of hypogene caves. Considering that mammillaries are deposited in shallower settings, contribution of shallow groundwater cannot be excluded (e.g., Temovski et al., 2022).

Phenomena such as recharge from the surface are expected to occur for a short time period. However, four manganese events in a 72 cm thick sample from Nychteridon Cave are incompatible with such a scenario because mammillaries are formed with quite low deposition rates (e.g., 0.7 µm $yr.^{-1}$ for Devil's Hole (Ludwig et al., 1992)). The role of surface input would have needed to have been intermittent for hundreds of thousands of years to have formed such mammillaries.

Source of Manganese and Formation Condition

In general, geothermal fluids potentially include manganese (Neupane and Wendt, 2017). Rock and mineral dissolution and volcanic activity can introduce manganese in the geothermal water. Biological activity may influence manganese content. Even meteoric water that carries manganese from soil and rocks can contribute to the content of deeper geothermal waters when they are mixed. In the studied caves from Lesvos Island, the volcanic activity of the island may have contributed to the manganese content of the geothermal waters. For Krya Vrysi Cave, an alternative source of manganese other than the geothermal water cannot be speculated upon with the available data. In Nychteridon Cave, the metallic oxide layers contain nickel that may come from ophiolites.

Substantial minor element content (such as nickel, cobalt, copper, and zinc) may be found in manganese oxides from caves (Frierdich and Catalano, 2012; White et al., 1985). The studied samples from mammillaries also host important minor elements (Table 2). Iron has co-precipitated in the manganese oxide layers of the studied mammillaries, whereas it was not detected in the manganese oxides of the Krya Vrysi Cave spars. Low values of Eh and pH control the mobilization of these metals, and higher values trigger their deposition. Iron oxides precipitate at pH > 6, whereas manganese oxides precipitate at pH > 8.5 (Hill and Forti, 1997; Onac, 1996). During manganese oxidation and subsequent deposition, acidification of the fluid due to the provided protons leads to corrosion of carbonates (Gázquez et al., 2012). This could explain the corrosion voids identified in sample Sp39. Among the analyzed samples, at least sample Sp39 was found to preserve biosignatures detected as a network of filaments. This supports the hypothesis that, at least in some cases, the overall process of corrosion may be microbially mediated (Moore, 1981; Cunningham et al., 1995; Northup et al., 2000; Spilde et al., 2005). Other minerals may also exist, such as the cerium-dominated one found in Sp16/4. However, they constitute less than 1% of the paragenesis, making their identification challenging.

Regional Effect on the Occurrence of Manganese Events

Considering the manganese events occurring within the speleothems formed during the latter stages of speleogenesis, it is essential to contextualize these occurrences within the broader geological process to decipher their significance. The caves under investigation belong to the category of endogenous hypogene caves, closely associated with geothermal fluids. This particular cave type, as described by Klimchouk (2017), is characterized by karstification occurring at significant depths or within upper hydrodynamic zones, where ascending flows follow structurally controlled pathways. In shallower settings, the precipitation of carbonates prevails due to a reduction in CO_2 partial pressure, as noted by Dublyansky (2013).

There exists a profound correlation between endogenous (hypogene) speleogenesis and the tectonic evolution of regions. This correlation allows the utilization of speleothems such as spar and mammillaries as indicators of the geological history and development of specific areas, as discussed by Polyak et al. (2014) and Polyak et al. (2008). Tectonic events, intrusions of magmatic substances, and related geological alterations can exert chemical influences on geothermal fluids and alter the pressure and temperature conditions conducive to carbonate deposition (e.g. Arnórsson, 1989; Dublyansky, 2000).

Hence, the conspicuous manganese events discernible within the carbonate minerals may serve not only as markers of manganese occurrences, but also as indicators of more extensive geological transformations on a relatively large scale. These events could be reflective of broader changes in the geological landscape influenced by tectonic forces, magmatic activities, and alterations in the geothermal fluid composition.

Future Research

Apart from the studied manganese events, the available data for the related carbonates are only indicative of the formation conditions (e.g., hydrothermal speleogenesis) and they do not provide evidence on how these systems evolved through time. More detailed investigation of a full series of these deposits could help identify if repetitions in the formation conditions exist or if the speleogenesis is a one-direction process.

CONCLUSIONS

The manganese events described are represented in at least 17 % of the carbonate phreatic speleothems of hydrothermal speleogenesis studied. They mark changes in the depositional system that influence the fluid chemistry in both shallow and deep phreatic conditions. Deposition of carbonates can be interrupted and dissolution may occur. The preserved biosignatures indicate that the process can be biologically mediated. The manganese events appear multiple times in the stratigraphy of mammillaries and in phantom crystals indicating a repetitive character. Time intervals between the manganese events are quite large based on the low rate of mammillary deposition. They are noticed in the phreatic speleothems of endogenous hypogene systems related to fluids of deep origin that flow along structural routes. Thus, if oscillatory systems are excluded, then large scale geological changes might be responsible for the occurrence of these events. Further study of the intermediate carbonate deposits in the future may provide more details for the nature of changes that are marked with the manganese events and how they are interpreted in terms of hypogene speleogenesis.

ACKNOWLEDGMENTS

Sampling was carried out under the authorization of the Ephorate of Paleoanthropology and Speleology, Greek Ministry of Culture and Sports. LG is grateful to cavers Lambros Makrostergios and Ilias Lambropoulos who provided information about the spar in Krya Vrysi Cave and guided him to the sampling site. We are grateful to the two anonymous reviewers for their invaluable suggestions, which have significantly enriched the quality of our manuscript.

REFERENCES

Allouc, J., and Harmelin, J.-G., 2001, Les dépôts d'enduits manganoferrifères en environnement marin littoral; l'exemple de grottes sous-marines en Méditerranée nord-occidentale [Ferromanganese deposits in shallow cryptic [sic] marine environment: Examples in [the] northwestern Mediterranean]: Bulletin de la Société Géologique de France, v. 172, p. 765–778, https://doi.org/10.2113/172.6.765.

Arnórsson, S., 1989, Deposition of calcium carbonate minerals from geothermal waters: Theoretical considerations: Geothermics, v. 18, p. 33–39, https://doi.org/10.1016/0375-6505(89)90007-2.

Carmichael, M.J., Carmichael, S.K., Santelli, C.M., Strom, A., and Bräuer, S.L., 2013a, Mn (II)-oxidizing bacteria are abundant and environmentally relevant members of ferromanganese deposits in caves of the upper Tennessee River Basin: Geomicrobiology Journal, v. 30, p. 779–800, https://doi.org/10.1080/01490451.2013.769651.

Carmichael, S.K,, and Bräuer, S.L., 2015. Microbial diversity and manganese cycling: A review of manganese-oxidizing microbial cave communities, *in* Engel, A.S., ed., Microbial Life of Cave Systems: Berlin, De Gruyter, p. 137–160, https://doi.org/10.1515/9783110339888-009.

Carmichael, S.K., Zorn, B.T., Santelli, C.M., Roble, L.A., Carmichael, M.J., and Bräuer, S.L., 2015, Nutrient input influences fungal community composition and size and can stimulate manganese (II) oxidation in caves: Environmental Microbiology Reports, v. 7, p. 592–605, https://doi.org/10.1111/1758-2229.12291.

Carmichael, S.K., Carmichael, M.J., Strom, A., Johnson, K.W., Roble, L.A., Gao, Y., and Bräuer, S.L., 2013b, Sustained anthropogenic impact in Carter Saltpeter Cave, Carter County, Tennessee, and the potential effects on manganese cycling: Journal of Cave and Karst Studies, v. 75, p. 189–204, https://doi.org/10.4311/2012MB0267.

Cunningham, K.I., Northup, D.E., Pollastro, R.M., Wright, W.G., and LaRock, E.J., 1995, Bacteria, fungi and biokarst in Lechuguilla Cave, Carlsbad Caverns National Park, New Mexico: Environmental Geology, v. 25, p. 2–8, https://doi.org/10.1007/BF01061824.

Decker, D.D., Polyak, V.J., Asmerom, Y., and Lachniet, M.S., 2018, U–Pb dating of cave spar: A new shallow crust landscape evolution tool: Tectonics, v. 37, p. 208–223, https://doi.org/10.1002/2017TC004675.

Dotsika, E., Poutoukis, D., Kloppmann, W., Guerrot, C., Voutsa, D., and Kouimtzis, T., 2010, The use of O, H, B, Sr, and S isotopes for tracing the origin of dissolved boron in groundwater in Central Macedonia, Greece, Applied Geochemistry, v. 25, p. 1783–1796, https://doi.org/10.1016/j.apgeochem.2010.09.006.

Dublyansky, Y.V., 2013, Karstification by Geothermal Waters, *in* Schroder, J., and Frumkin, A., eds., Treatise on Geomorphology, v. 6, Karst Geomorphology: San Diego, Academic Press, p. 57–71, https://doi.org/10.1016/B978-0-12-374739-6.00110-X.

Dublyansky, Y.V., 2000, Hydrothermal speleogenesis: Its settings and peculiar features, *in* Klimchouk, A.B., Ford, D.C., Palmer, A.N., and Dreybrodt, W., eds., Speleogenesis: Evolution of karst aquifers: Huntsville, National Speleological Society, p. 292–297, https://www.researchgate.net/publication/267410370_Hydrothermal_Speleogenesis-_Its_Settings_and_Peculiar_Features.

Frierdich, A.J., and Catalano, J.G., 2012, Distribution and speciation of trace elements in iron and manganese oxide cave deposits: Geochimica et Cosmochimica Acta, v. 91, p. 240–253, https://doi.org/10.1016/j.gca.2012.05.032.

Frierdich, A.J., Hasenmueller, E.A., and Catalano, J.G., 2011, Composition and structure of nanocrystalline Fe and Mn oxide cave deposits: Implications for trace element mobility in karst systems: Chemical Geology, v. 284, p. 82–96, https://doi.org/10.1016/j.chemgeo.2011.02.009.

Gázquez, F., Calaforra, J.M., and Forti, P., 2011, Black Mn-Fe crusts as markers of abrupt palaeoenvironmental changes in El Soplao Cave (Cantabria, Spain): International Journal of Speleology, v. 40, p. 163–169, https://doi.org/10.5038/1827-806X.40.2.8.

Gázquez, F., Calaforra, J.-M., and Rull, F., 2012, Boxwork and ferromanganese coatings in hypogenic caves: An example from Sima de la Higuera Cave (Murcia, SE Spain): Geomorphology, v. 177–178, p. 158–166, https://doi.org/10.1016/j.geomorph.2012.07.022.

Gradziński, M., Banaś, M., and Uchman, A., 1995, Biogenic origin of manganese flowstones from Jaskinia Czarna Cave, Tatra Mts., Western Carpathians: Annales Societatis Geologorum Poloniae, v. 65, p. 19–27, http://asgp.pl/sites/default/files/volumes/65_1-4_019_027.pdf.

Hill, C.A., and Forti, P., 1997, Cave Minerals of the World, 2nd ed.: Huntsville, National Speleological Society, 463 p.

Jones, B., 1992, Manganese precipitates in the karst terrain of Grand Cayman, British West Indies: Canadian Journal of Earth Sciences, v. 29, p. 1125–1139, https://doi.org/10.1139/e92-091.

Klimchouk, A., 2017, Types and settings of hypogene karst, *in* Klimchouk, A., Palmer, A.N., De Waele, J., Auler, A.S., and Audra, P., eds., Hypogene Karst Regions and Caves of the World: Cham, Switzerland, Springer, p. 1–39, https://doi.org/10.1007/978-3-319-53348-3_1.

Lazaridis, G., 2009, Petralona Cave: Morphological analysis and a new perspective on its speleogenesis, *in* Hypogene Speleogenesis and Karst Hydrogeology of Artesian Basins Institute of Speleology and Karstology, Simferopol, Ukraine, special paper 1, p. 233–239, https://www.researchgate.net/publication/315457290_PETRALONA_CAVE_MORPHOLOGICAL_ANALYSIS_AND_A_NEW_PERSPECTIVE_ON_ITS_SPELEOGENESIS.

Lazaridis, G., 2017, Hypogene speleogenesis in Greece, *in* Klimchouk, A., Palmer, A.N., De Waele, J., Auler, A.S., and Audra, P., eds., Proceedings: Hypogene Karst Regions and Caves of the World, Cham, Switzerland, Springer, p. 225–239, https://doi.org/10.1007/978-3-319-53348-3_14.

Lohnert, E., and Papakonstntinou, A., 1988, Relationship between karst and porous aquifers on Chalkidiki Peninsula, Greece, Proceedings of the IAH 21st Congress, v. XXI, part 1, Gulin, China, p. 321–326.

Ludwig, K.R., Simmons, K.R., Szabo, B.J., Winograd, I.J., Landwehr, J.M., Riggs, A.C., and Hoffman, R.J., 1992, Mass-spectrometric ^{230}Th-^{234}U-^{238}U dating of the Devils Hole calcite vein: Science, v. 258, p. 284–287, https://doi.org/10.1126/science.258.5080.284.

Moore, G., 1981, Manganese deposition in limestone caves, *in* Beck, B.F., ed., Proceedings of the 8th International Congress of Speleology, v. 2, Bowling Green, Kentucky, National Speleological Society, p. 642–644.

Neupane, G., and Wendt, D.S., 2017, Assessment of mineral resources in geothermal brines in the US, *in* Proceedings, 42nd Workshop on Geothermal Reservoir Engineering, Stanford, Cal., Stanford Geothermal Program, p. 1490–1507, https://www.researchgate.net/publication/313904235_Assessment_of_Mineral_Resources_in_Geothermal_Brines_in_the_US.

Northup, D.E., Dahm, C.N., Melim, L.A., Spilde, M.N., Crossey, L.J., Lavoie, K.H., Mallory, L.M., Boston, P.J., Cunningham, K.I., and Barns, S.M., 2000, Evidence for geomicrobiological interactions in Guadalupe caves: Journal of Cave and Karst Studies, v. 62, p. 80–90, https://caves.org/wp-content/uploads/Publications/JCKS/v62/cave_62-02-fullr.pdf.

Oikonomidis, G., Charalampidis, C., Dimitraki, D., Varis, A., and Polydoropoulos, K., 2022. Exploration of a newly discovered cave section: the case of Nychteridon Cave, Chalkidiki, Greece. Proceedings of the 18th International Congress of Speleology - Savoie Mont Blanc 2022, Vol. II - Karstologia Mémoires n°22 - SYMPOSIUM 02 - Caving and Explorations, 157-160.

Onac, B.P., 1996, Mineralogia speleotemelor din unele peşteri ale Munţilor Pădurea Craiului, cu referiri asupra semnificaţiei lor paleoclimatice [Mineralogy of speleothems from caves in the Pădurea Craiului Mountains and their palaeoclimatic significance] [Ph.D. thesis], Universitatea Babeş-Bolyai, 185 p.

Onac, B.P., Pedersen, R.B., and Tysseland, M., 1997, Presence of rare-earth elements in black ferromanganese coatings from Vântului Cave (Romania): Journal of Caves and Karst Studies, v. 59, p. 128–131, https://caves.org/wp-content/uploads/Publications/JCKS/v59/cave_59-03-fullr.pdf

Papier, S., Baele, J.-M., Gillan, D., Barriquand, L., and Barriquand, J., 2011, Manganese geomicrobiology of the black deposits from the Azé Cave, Saône-et-Loire, France: Quaternaire, hors-série 4, p. 297–305, https://www.researchgate.net/publication/252628925_Manganese_geomicrobiology_of_the_black_deposits_from_the_az_cave_sane-et-loire_France.

Peck, S.B., 1986, Bacterial deposition of iron and manganese oxides in North American caves: NSS Bulletin, v. 48, p. 26–30, https://caves.org/wp-content/uploads/Publications/Bulletin/Vol%2048%20num%201.pdf.

Polyak, V., Hill, C., and Asmerom, Y., 2008, Age and evolution of the Grand Canyon revealed by U-Pb dating of water table-type speleothems: Science, v. 319, p. 1377–1380, https://doi.org/10.1126/science.1151248.

Polyak, V., Asmerom, Y., Hill, C.A., Palmer, A.N., Provencio, P.P., Palmer, M.V., McIntosh, W.C., Decker, D.D., and Onac, B.P., 2014, Isotopic studies of byproducts of hypogene speleogenesis and their contribution to the geologic evolution of the western United States, *in* Proceedings, Hypogene Cave Morphologies, San Salvador Island, Bahamas: Leesburg, Va., Karst Waters Institute, special publication 18, p. 88–96, https://karstwaters.org/wp-content/uploads/2015/04/SP18_Hypogene1.pdf.

Rossi, C., Lozano, R.P., Isanta, N., and Hellstrom, J., 2010, Manganese stromatolites in caves: El Soplao (Cantabria, Spain): Geology, v. 38, p. 1119–1122, https://doi.org/10.1130/G31283.1.

Spilde, M.N., Northup, D.E., Boston, P.J., Schelble, R.T., Dano, K.E., Crossey, L.J., and Dahm, C.N., 2005, Geomicrobiology of cave ferromanganese deposits: A field and laboratory investigation: Geomicrobiology Journal, v. 22, p. 99–116, https://doi.org/10.1080/01490450590945889.

Tarassov, M., Janakieva, Z., and Tarassova, E., 2017, Phantom crystals of pyrite from the Yuzhna Petrovitsa deposit, Madan ore field, Bulgaria, Bulgarian Geological Society, *in* Proceedings, National Conference with International Participation “Geosciences 2017”, Sofia: Bulgarian Geological Society, p. 37–38, https://www.researchgate.net/publication/321886579_Phantom_crystals_of_pyrite_from_the_Yuzhna_Petrovitsa_deposit_Madan_ore_field_Bulgaria.

Temovski, M., et al., 2022, Combined use of conventional and clumped carbonate stable isotopes to identify hydrothermal isotopic alteration in cave walls: Scientific Reports, v. 12, article 9202, 16 p., https://doi.org/10.1038/s41598-022-12929-4.

Thomaidou, E.L., 2009, I geologikí domí tis nísou Lésvou [Geological structure of Lesvos Island] [PhD. Thesis], Aristotle University of Thessaloniki, 200 p., https://ikee.lib.auth.gr/record/122648/files/Thomaidou_Efi.pdf.

Veni, G., Poulianos, N., Golobovic Deligianni, M., and Poulianos, A.N., 2009, Preliminary hydrogeologic survey of Petralona Cave, Chalkidiki, Greece, *in* Proceedings of the 15th International Congress of Speleology, v. 3, Kerrville, Texas, International Union of Speleology, p. 1717-1722, https://digitalcommons.usf.edu/cgi/viewcontent.cgi?article=1010&context=kip_talks.

White, W.B., Scheetz, B.E., Atkinson, S.D., Ibberson, D., and Chess, C.A., 1985, Mineralogy of Rohrer’s Cave, Lancaster County, Pennsylvania, NSS Bulletin, v. 47, p. 17–27, https://caves.org/wp-content/uploads/Publications/Bulletin/Vol%2047%20num%201.pdf

Olga Y. Chervyatsova, Nikolay N. Grigoryev, Ludmila Y. Kuzmina, Yuri V. Dublyansky, Rayan T. Akhmedyanov, and Sergey S. Potapov. Documentation of a sudden Karstic Lake Drainage Event in the Shulgan River Valley (Southern Ural, Russia). *Journal of Cave and Karst Studies*, v. 87, no. 1, p. 13-28. DOI:10.4311/2023ES0103

DOCUMENTATION OF A SUDDEN KARSTIC LAKE DRAINAGE EVENT IN THE SHULGAN RIVER VALLEY (SOUTHERN URAL, RUSSIA)

Olga Y. Chervyatsova,[1,C] Nikolay N. Grigoryev,[2] Ludmila Y. Kuzmina,[2,3] Yuri V. Dublyansky,[4] Rayan T. Akhmedyanov,[2] and Sergey S. Potapov[5]

ABSTRACT

This article presents hydrological, hydrogeochemical, and mineralogical features of karstic lakes located in the basin of the disappearing, karstic Shulgan River (southern Ural, Russia). The lakes are currently isolated from karstic channels by bottom sediments; for several decades, their levels were relatively stable. We document a case of a "breakthrough" drainage event (occurring approximately once every 50 years), which occurred in 2021–2022 and the subsequent recovery of one of the lakes, Lake Ygyshma. Thanks to hydrological monitoring at the Goluboe Ozero spring and in the Shulgan-Tash Cave, it was possible to record the time of the breakthrough and the time of lake water transit, confirming the hydrogeological connection between lakes and the underground Shulgan River. This paper proposes a conceptual model of the evolution of isolated karstic lakes and the formation of the unconventional (for epigenic carbonate karst) hydrogeochemical characteristics in them (enrichment with metals, gases, etc.).

INTRODUCTION

Karstic lakes are a common surface-karst feature. The character of water exchange in karstic lakes may differ significantly. Lakes that retain an active hydrodynamic connection with the karstic waters of the phreatic zone are characterized by pronounced seasonal water level fluctuations and may disappear in low-water years or seasons of the year (Andrić and Bonacci, 2014; Bonacci et al., 2014; McCormack et al., 2017; Sironić et al., 2017). For example, for "disappearing" lakes of Slovenian karst, acts of filling and drainage are recorded one to five times a year (Ravbar et al., 2021). The hydrological regime of such reservoirs is well understood, in particular, due to the use of modeling methods (Mayaud et al., 2019, 2022).

At the other end of the spectrum lie karstic lakes that have lost their connection to karstic waters due to occlusion of karstic conduits by sediments (isolated lakes). Recharge of such lakes is primarily by atmospheric precipitation, with epikarstic flow and groundwater playing auxiliary roles (Kindinger et al., 1999). For lakes of this type, episodes of sudden lowering of the water level, up to complete drying, are sometimes observed. Such episodes are caused by degradation of sediment plugs and restoration of hydraulic connection between the lake and the karst conduits. Disappearances of lakes are often unrelated to the precipitation regime, occur unexpectedly, and are much rarer. Some of these cases have been the subject of multidisciplinary studies (Roningen and Burbey, 2012; Bücker et al., 2021; Leal-Bautista et al., 2021; Tizzard and Horne, 2021).

Documentation of disappearance of isolated karstic lakes is usually hampered by the lack of hydrological monitoring. This does not allow for accurately establishing the time and dynamics of the event, as well as understanding the relationship with underground karstic systems and determining the location of drained water discharge. In this paper we describe details of the disappearance and subsequent refilling of an isolated karstic lake in southern Ural. For the first time we were able to obtain a hydrological record of the breakthrough of the isolated Lake Ygyshma (occurring approximately once every 50 years), the transit of water through the karstic system, and its discharge from a karst spring 2.8 km from the lake.

A separate focus of the study was the geochemical and mineralogenetic processes occurring in isolated karstic lakes, leading to the formation of specific geochemical characteristics of water and lake bottom sediments, dissimilar from typical conditions of epigenic karst. Such studies have been conducted for wetland conditions (Furukawa and Takahashi, 2008; Johnson et al., 2012; and Guseva, 2016, etc.); we have not found similar publications on isolated karstic lakes.

[1] Shulgan-Tash State Natural Biosphere Reserve, Zapovednaya 14, Irgyzly, Burzyansk District, Bashkortostan Republic, 453585 Russia
[2] Historical and Cultural Museum-Reserve "Shulgan-Tash Cave," Chernyshevskogo, 47, Ufa, Bashkortostan Republic, 450076 Russia
[3] Ufa Institute of Biology of the Ufa Federal Research Center of the Russian Academy of Sciences, Prospect Octyabrya 69, Ufa, Bashkortostan Republic, 450054 Russia
[4] Leopold-Franzens-Universität Innsbruck, Institute für Geologie, Innrain 52, Innsbruck, 6020 Austria
[5] South Urals Research Center of Mineralogy and Geoecology, Ural Branch of the Russian Academy of Sciences, Miass, Chelyabinsk Oblast, 456317 Russia
[C] Corresponding author: kittary@yandex.ru

STUDY AREA

Physiography

The study area is located within the west Ural outer folding zone, at heights of 400–600 m, and belongs to the basin of the disappearing, karstic Shulgan River (Abdrakhmanov et al., 2002). The area is characterized by rolling hilly relief with individual ridges composed of terrigenous-carbonate rocks. Most of the area is covered with mixed broad-leaved (linden, elm maple), and light coniferous/small-leaved (pine, birch, aspen) forests growing on gray mountain-forest and sod-carbonate soils.

Climate

The area is located in a zone of moderate continental climate with excessive moisture (Dfb according to the Köppen-Heiger classification: cold continental, without dry season, with warm summer). The mean air temperature is 0.9 °C, with maximum mean monthly temperatures recorded in July (17 °C) and minimums in January (–16 °C). The mean annual precipitation is 550 mm; about two-thirds of it falls in summer.

Geology

The study area is located within the southern miogeosynclinal Paleozoic rim of the Bashkirian meganticlinorium. The Shulgan River basin is developed within the north-northeastern-oriented Irgizlinskaya Syncline. The syncline is built up of carbonate rocks of Paleozoic age, deposited with angular unconformity on Late Proterozoic sediments (siltstones, mudstones, sandstones, dolomites, etc.; Knyazev et al., 2015). Most of the area is mantled by Quaternary deposits 4–30 m thick.

Hydrology and Hydrogeology

The sinking, karstic Shulgan River is a tributary of the Belaya River. The Shulgan River basin extends in north-south direction for 12.5 km occupying an area of 45.8 km^2, of which 30.6 km^2 are karstifiable rocks. Some 7.5 km downstream of the source, the Shulgan River is swallowed by the entrance sinkhole of the Ozhiganova Cave. South of this point the Shulgan valley is waterless (Fig. 1A) and surface flow is observed only during extreme floods. About 0.5 km downstream of the Ozhiganova sinkhole, the waterless Northern Valley joins the Shulgan Valley. Further south the Shulgan Valley is joined by several second-order dry valleys, featuring numerous karstic sinkholes that redirect the surface runoff underground.

The water of the Shulgan River emerges in the Shulgan-Tash (Kapova) Cave (Fig. 1A, B). The cave comprises a series of large halls, galleries and interconnected steep passages, organized in a three-dimensional structure. The mapped length of the cave is 3,123 m, 2,323 m of which is above the water table and the remaining 800 m is represented by phreatic-zone passages (Lyakhnitsky et al., 2013). The Shulgan River emerges from a siphon in the northern part the cave and flows through several galleries and halls, separated by 5–6 m deep siphons. At the southern end of the Chasm Hall, the river plunges into deep phreatic gallery (explored to a depth of 82 m). The river re-emerges in the Vauclusian spring called Blue Lake in the entrance hall of the cave (Fig. 1C). Two hundred meters downstream from the resurgence, the Shulgan River eventually flows into the Belaya River (Fig. 1A). The low-water discharge of the Shulgan River at Blue Lake does not exceed 0.3 $m^3 s^{-1}$, increasing up to 5–6 $m^3 s^{-1}$ during the spring snowmelt floods.

Five karstic lakes, Fatima, Ollukul, Yylkysykkan, Dvoinoye, and Ygyshma, are present in the dry Shulgan Valley 150–660 m south of the entrance sinkhole of the Ozhiganova Cave. The last two lakes are located at the junction of the Shulgan and Northern Valleys (Fig. 2). Two of the lakes, Fatima and Dvoinoye, are degraded to the stage of a peat bog.

MATERIALS AND METHODS

The digital maps were constructed using the Global Mapper v. 19 software (Blue Marble Geographics) from a digital elevation model created by airborne laser scanning in 2018 (Svoyskiy et al., 2020; Shulgan-Tash Cave Museum-Reserve, 2020). The digital model of the Lake Ygyshma basin was created by photogrammetric method using RealityCapture v. 1.0 beta software (Capturing Reality, now Epic Games, Inc.). Further data analysis (mapping, volume calculation, etc.) was carried out using Geomagic Wrap 2017 software (3D Systems Corp.) and Global Mapper. The volume of displaced landslide material was estimated using Geomagic Wrap. A polygonal model of the landslide body was built (based on its apparent thickness) and the volume of the model was calculated using the calculate volume tool. A Fluke Ti300 thermal imager and Fluke SmartView Classic 4.4 software were used for infrared mapping.

The hydrological regime of Shulgan River was monitored at two monitoring stations: the Blue Lake Spring and Chasm Hall of Shulgan-Tash Cave (Fig. 1B). An LTC Levelogger Edge M20-C80 logger (level, temperature, conductivity) (Solinst Canada Ltd.) was used at the Blue Lake (monitoring station 1), and an LT Levelogger Edge M30 (level, temperature) (Solinst Canada Ltd.) was used at Chasm Hall (monitoring station 2). The measurement error was ±0.05 % for the level, ±0.05 °C for the temperature, and ±1 % for the conductivity. Compensation of barometric fluctuations was performed using data from the LT Barologger Edge M 1.5 logger (Solinst Canada Ltd.). All loggers were synchronized and measurements were performed every 30 minutes.

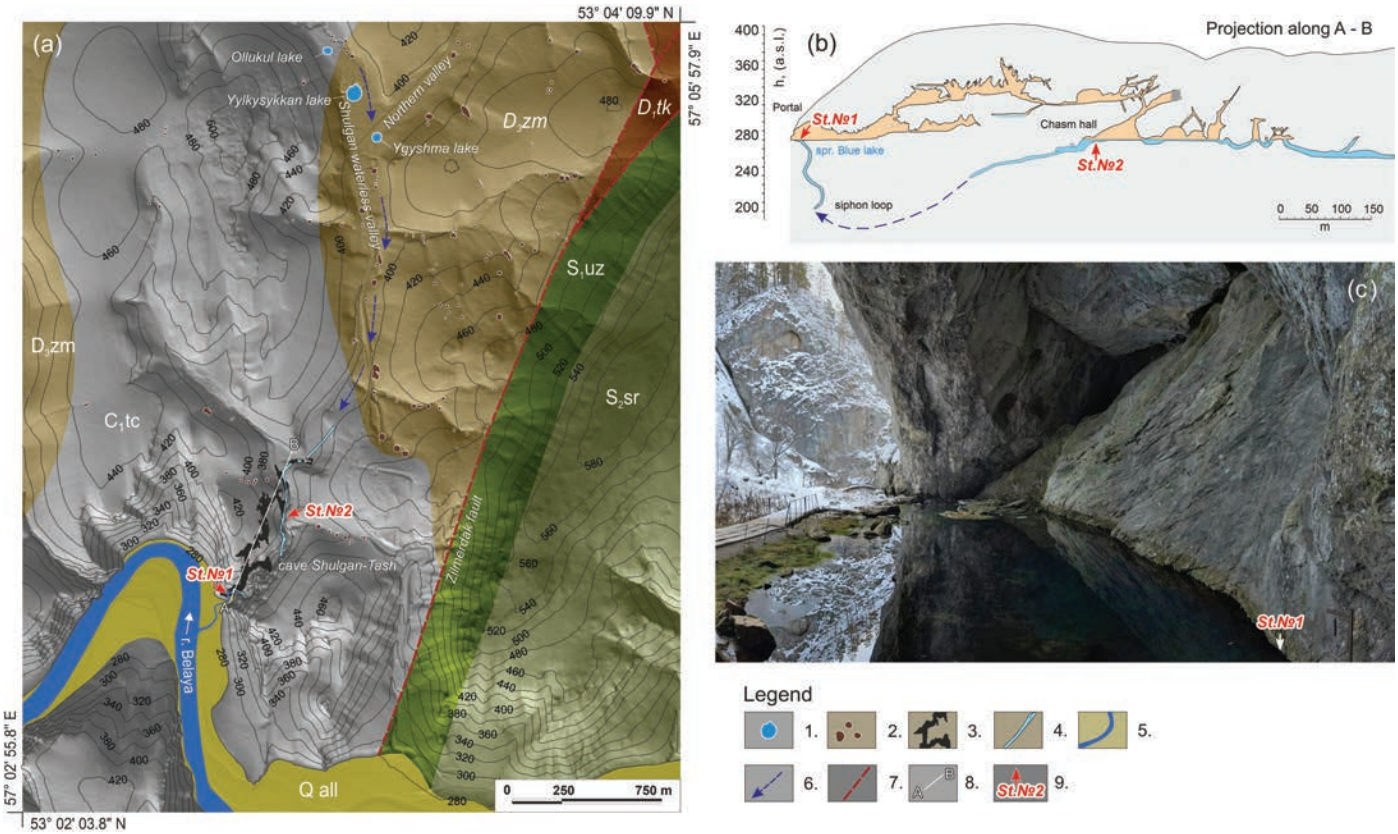

Figure 1. Study area. (A) Map of the study area with superimposed geological information and projection of Shulgan-Tash Cave. Digital relief model is by Svoyskiy et al. (2020). Geology is modified from Knyazev et al. (2015). Elevation contours are labeled in m a.s.l. (Baltic system of elevation). (B) Projection of Shulgan-Tash Cave along line A–B and legend no. 8 in Fig. 1A. (C) Vauclusian Blue Lake Spring in the entrance hall of Shulgan-Tash Cave, discharging waters of the Shulgan River.

Legend for the map in Fig. 1A. (1) Karstic lakes. Only open water surfaces, as of 2022, are shown. For lakes turned into peat bogs, see Fig. 2. (2) Swallowing sinkholes. (3) Projection of Shulgan-Tash Cave. (4) Cave galleries hosting the underground flow of the Shulgan River. (5) Permanent surface watercourses. (6) Infrared underground water flow directions. (7) Large tectonic fault. (8) Line of cave projection shown in Fig. 1*B*. (*9*) Monitoring stations in Fig.1A–C.

Stratigraphic units shown in Fig. 1A. (C_1tc) Terrigenous-carbonate sequence; limestone, >150 m. (D_3zm) Zilimskaya series; limestone, up to 350 m. (D_1tk) Takatinskaya Formation; quartz sandstone, gravelite, 200 m. ($D_{1–3}$bl) Belskaya Formation; limestone, layers of quartz sandstone, siltstone, and dolomite, 1000–1200 m. (S_2sr) Sermenevskaya Formation, dolomite, limestone, layers of siltstone, 500 m. (S_1uz) Uzyanskaya Formation; argillite, layers of siltstone and clayey limestone, 150–300 m.

Temperature, conductivity, and pH of the water were measured using a HI98194 meter (Hanna Instruments). The ionic composition of water was determined using titrimetric (HCO_3^-, Cl^-, Ca^{2+}, Mg^{2+}; uncertainty ca. 5%) and photocolorimetric (SO_4^{2-}; uncertainty ca. 10 %) methods. The total content of sodium and potassium ions was assessed from the difference between the sums of the anions and the cations (Nazarova and Boeva, 2002).

Calculation of saturation indices for different minerals was carried out using the Aqion v. 6.7.3 software. Saturation indices for calcite, siderite, and iron (oxy) hydroxide were calculated for two scenarios: a “closed system,” envisaging mineral formation in water column, and an “open system” (in equilibrium with atmospheric air at a carbon dioxide concentration of 420 ppm), simulating mineral formation in the surface water layer of outflowing springs.

Microscopic examination of mineral samples was carried out using a DM 1000 light microscope equipped with a DFC-290 digital camera (Leica Microsystems). The morphology and elemental composition of minerals were investigated using a Vega 3 scanning electron microscope (SEM) (Tescan) equipped with an X-ACT energy-dispersive X-ray spectrometer (EDS) (Oxford Instruments) and using a Mira 3 scanning electron microscope (Tescan). Identification of mineral species was based on elemental composition and the proximity of the calculated empirical formulas to stoichiometric values in the ideal formulas. The formulae were calculated by the oxygen method using the MineralCalc v. 1.1 software (https://petroexplorer.ru). Statistical analysis of the data was carried out using the PAST 4.0 software (Hammer et al., 2001) and Microsoft Excel software.

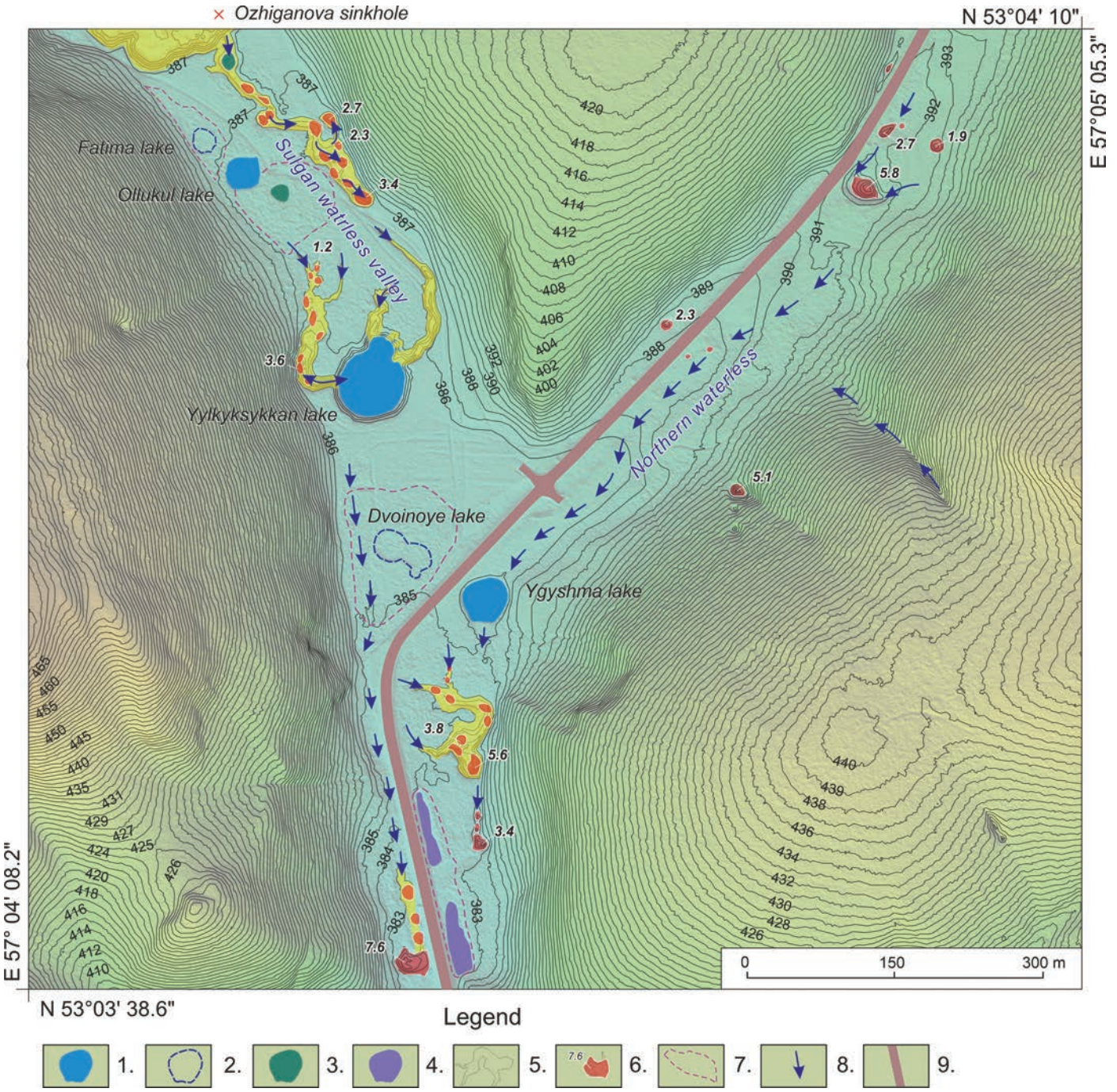

Figure 2. Map of karstic lakes in the Shulgan Valley. Elevation contours are marked in m a.s.l. (Baltic system of elevation). *Legend*: (1) Open (with open water surface lakes). (2) Lakes converted to peat bogs (the water surface is covered with peat floating mats). (3) Ephemeral lakes (as of May 2018). (4) Technogenic reservoirs. (5) Erosional incisions of flood watercourses (blind karstic ravines). (6) Swallowing sinkholes and their depth in meters. (7) Wetland areas. (8) Directions of flood watercourses. (9) Road.

RESULTS

Karstic Lakes in the Shulgan River Basin

In the first descriptions dating back to 1923 and 1968, the number of karstic lakes in the Shulgan River basin varied between eight (Vakhrushev, 1960) and five (Kudryashov, 1969). Only three lakes, Yylkysykkan, Ygyshma, and Ollukul, are mentioned in publications and archive materials dating between 1985 and 2016. (Lyakhnitsky and Shchelinsky, 1987; Lyakhnitsky and Chuiko, 2001; Kuzmina et al., 2013; Chervyatsova et al., 2015; Shulgan-Tash State Natural Biosphere Reserve, 1985–2016). Early bathymetric data (Kudryashov, 1969) show maximum depths of the lakes ranging from 16.5 m through 36.7 m. Our measurements in 2009 and 2022 showed that the depths of the lakes had decreased

Table 1. Karst lakes known in the Shulgan river basin.

Lake	Center Point Coordinates (WGS-84)	Shape	Dimensions [m] (as of 05/2018)	Surface Area [m²] (as of 05/2018)	Maximum Depth [m]	Volume [m³]
Fatima (peat bog)	N 53° 04′ 06.4″ E 57° 04′ 18.12″	circular	23 × 25	377	...	...
Ollukul	N 53° 04′ 05.3″ E 57° 04′ 20.3″	circular	38 × 36	935	23.0 (1968) 6.7 (2022)	2,060 (2022)
Yylkyksykkan	N 53° 03′ 58.45″ E 57° 04′ 27.23″	oblong	83 × 62	3,700	36.7 (1968) 15.5 (2009)	20,095 (2009)
Dvoinoye (peat bog)	N 53° 03′ 52.91″ E 57° 04′ 29.1″	complex, consisting of several rounded sinkholes	55 × 23	1,160	...	...
Ygyshma	N 53° 03′ 51.31″ E 57° 04′ 33.52″	circular	47 × 44	1,616	16.5 (1968) 10.7 (2009)	7,769 (2009)

substantially (Table 1). The bathymetry of Lakes Yylkysykkan and Ollukul is shown in Supp. Fig. S1. The basin of Lake Ygyshma has an asymmetrical, conical shape with steep northeastern and gentler southwestern slopes.

Analysis of aerial photographs, a digital elevation model, and field observations reveal that, in addition to open water bodies, there are two more lakes on the site that are now completely covered by peat, i.e., that have turned into typical peat bogs (Volkova et al., 2010). One such lake, for which it was possible to restore the local name Fatima (Aigul Sharafutdinova, public relations officer from the Shulgan-Tash Cave Historical and Cultural Museum-Reserve, personal communication, 2021), is located 22 m northwest of Lake Ollukul (Fig. 2, Supp. Fig. S2). The second lake/peatbog, provisionally named Dvoinoye (Double), is located 43 m northwest of Lake Ygyshma (Fig. 2, Supp. Fig. S2). It has a complex shape and appears to be formed by several coalesced sinkholes. On aerial photographs taken in 1959, both lakes had an open water surface which may explain differences in number of lakes mentioned in Vakhrushev (1960) and Kudryashov (1969) and in recent studies. Morphometric data of the lakes are summarized in Table 1.

The lakes of the Shulgan River basin, its sinkholes, the direction of flood flows, and the related erosion network are shown in Figure 2. In addition to perennial lakes, ephemeral lakes periodically appear in the valley. They form in shallow karstic sinkholes whose ponors become clogged by sediments. The depth of such lakes rarely exceeds 1.5–2.0 m; they usually do not exist more than two to three years. There are in addition two artificial reservoirs with a total area of 1900 m² located 180 m south of Lake Ygyshma. They appeared in 1970 as a result of changes in the natural surface flow caused by the construction of a highway.

None of the karstic lakes in the Shulgan River basin have outflows. Their recharge by surface flow is possible only during spring snowmelt floods (April to May). During the rest of the year, the runoff is completely absorbed by sinkholes higher up the valley. According to observations from 2008 to 2022, the level of Lakes Yylkysykkan and Ygyshma decreased by 1.0–1.5 m during the winter low-water period, while the level of Lake Ollukul remained relatively stable. In the area shown on Figure 2, the karstifiable limestone (Zilimskaya series) is mantled by 2.5–3.6 m thick layer of Middle Pleistocene to Holocene deposits (gravely and sandy siltstones; Knyazev et al., 2015). Based on the elevation of siphons in Ozhiganova Cave, the karstic water table is at a depth of ca. 38 m below land surface (Tkachev, 1999). The connection between Ozhiganova Cave and the karstic hydrosystem of the underground Shulgan River was previously established using a tracer test (Kudryashov, 1969).

Draining and Replenishment of Lake Ygyshma in 2021–2022

Episodes of rapid (within several hours) complete drainage are known for Lake Ygyshma. Two such episodes occurred in the last century, in 1921 and 1975 (Michael Kosarev, Shulgan-Tash State Natural Biosphere Reserve director, personal communication, 2021). The last disappearance of the lake, which became the focus of our study, happened on the night of September 27–28, 2021 (Supp. Fig. S3). After the lake disappeared, a logjam of sunken wood (local birch, aspen, and linden species) was found at the exposed bottom of the lake. Many trunks had traces of sawing or felling. This suggests that the decrease of the lake depths between 1968 and recent times (Kudryashov, 1969) may be due to pollution of lakes by anthropogenic timbering activity (timber deposits in the bottom part of sinkholes can be several meters thick).

During and after draining of the lake basin in 2021, landslide processes were activated within it. In a peripheral zone of the basin, with slopes of 17°–25°, intact sediments were not affected (Fig. 3A). At depths of 1.8–3.4 m, there is a cliff below which the basin walls become steeper; in this area soft deposits slid down under the force of gravity. In the lower part of the basin, the northeastern slopes

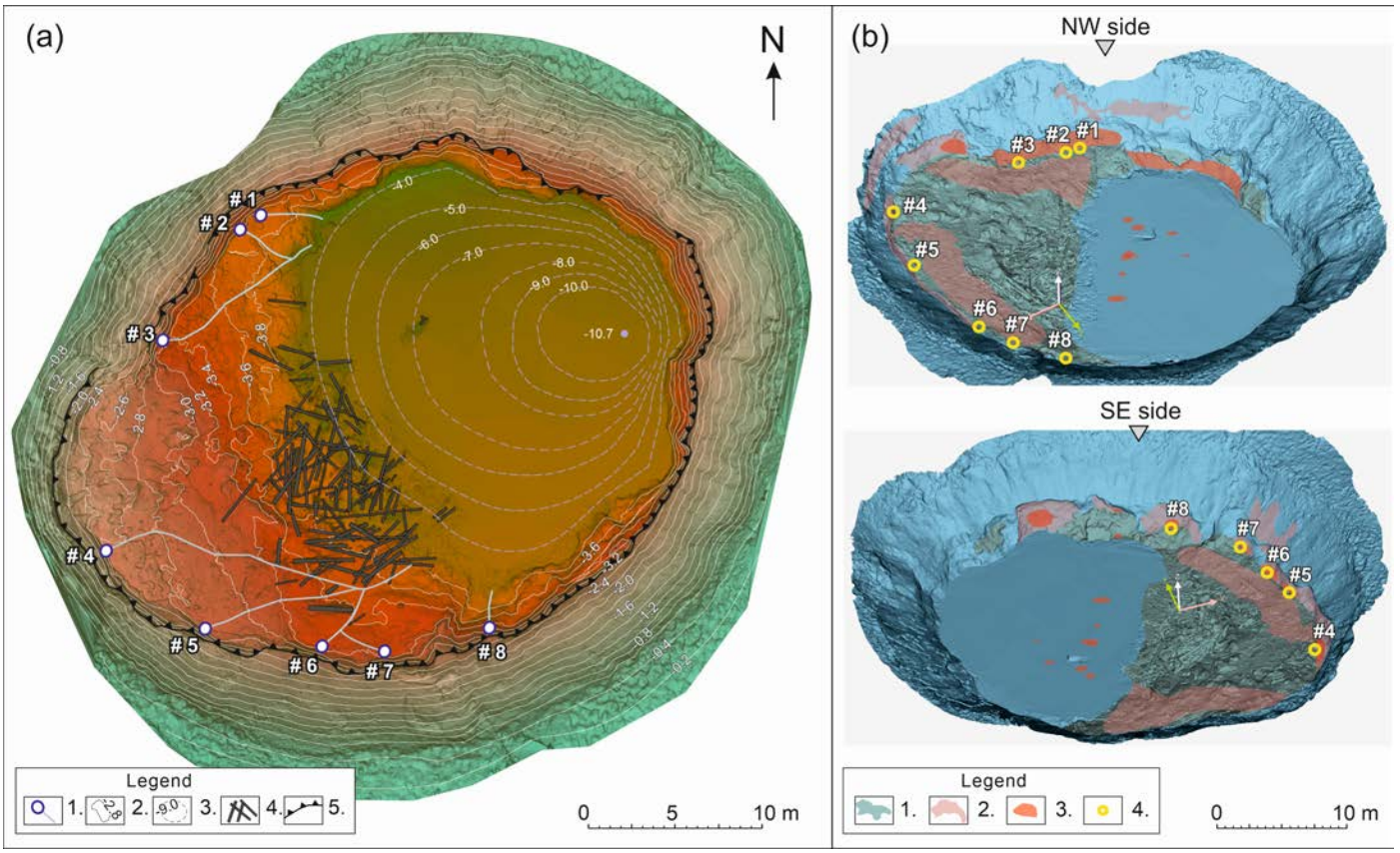

Figure 3. Views of the Lake Ygyshma basin based on the authors' photogrammetric model. (A) Plan view. Legend: (1) Eight numbered springs. (2) Above-water contours at 0.2 m (zero datum is the July 2009 water level). (3) Underwater isobaths at 1 m, based on 2009 measurements. (4) Submerged timber. (5) Cliff edge caused by lake sediments detachment and movement.

(B) Views looking down and to the northwest (*top*) and down and to the southeast (bottom) showing thermal anomalies revealed by infrared imaging superimposed on the digital elevation model. Vertical scale exaggeration 2×. Legend: (1) Activated landslide bodies. (2) Weak thermal anomalies. (3) Strong thermal anomalies. (4) Numbered springs.

are steeply inclined (60°–70°) or near vertical, and the southwestern slopes show gentler inclination. In the western part of the basin, a landslide body has formed covering an area of ca. 400 m^2. Comparison of images taken on September 28 and October 18, 2022 (Fig. 4A, Supp. Fig. S3), indicates that landslides occurred after the lake was drained. The volume of the material displaced at this stage, estimated from the photographs and the digital model, was at least 800 m^3. The development of gravitational processes, especially on the steep northern and northeastern lake sides, intensified in the springtime under the influence of freeze-thaw activity and solifluction.

The water which left Lake Ygyshma during this sudden drainage event passed through unidentified underground passages, emerged in Shulgan-Tash Cave, sunk again in a syphon, and re-emerged in the Blue Lake Spring. Here we try to assess the time that was needed for this. Dataloggers installed in an underground river in the Shulgan-Tash Cave (monitoring station 2) and in the Blue Lake (monitoring station 1; see Supp. Mat. 2) recorded virtually simultaneous transient increases of the water level (and, correspondingly, of the flow rate) on September 28, 2021, between 00:00 hours and 00:30 hours local time (GMT +5). Meanwhile, the water temperature and electrical conductivity of water at these two stations remained unchanged. These parameters changed, recording arrival of actual lake water, after 2.5 d. (60.5 hr at station 2) and 5.5 d. (132 hr at station 1) (Supp. Fig. S7; Supp. Table S2).

Synchronous registration of transient water flow peaks at both stations, separated by 650 m of deep (>80 m) siphon channels, indicates that the peaks were caused by piston action (i.e., by "pushing" phreatic water through the system). Because of the distance and depth of the siphon channels separating the two stations, an extremely high transmission rate of this pressure signal can be inferred. Considering this high velocity of propagation of the hydraulic signal through the system, we consider that the time of the appearance of the signal at monitoring stations closely corresponds to the time of the breakthrough of the lake bottom sediments and commencement of abrupt lake drainage. The phreatic flow velocity between Lake Ygyshma and the Shulgan-Tash Cave is estimated at ca. 0.01 m s^{-1}, and between the inner part of the cave and the Blue Lake Spring, ca. 0.003 m s^{-1} (Supp. Table S2).

The recovery of the lake began almost immediately after its drainage. On September 30, 2021, eight springs opened on the southern and western slopes of the lake reservoir (Fig. 3). The springs were confined to a landslide body and had

Figure 4. Springs opened in the basin of the drained Lake Ygyshma. (A) General view of the landslide body in the western part of the lake basin and the positions of springs (arrows). (B) Outlet of one of the springs on the southwestern slope of the basin. (C) Stream from the spring in Fig. 1B. The orange color is due to deposits of iron (oxy) hydroxides.

discharges of 0.1–1.0 L s^{-1}. In the first days after drainage, the lake filling rate exceeded 100 m^3 d^{-1}, but by June 2022 it had decreased to ca. 5.7 m^3 d^{-1} (Fig. S4, Supp. Table S1).

Additional information about the discharge of ground and karstic waters into the lake basin is given by the results of infrared surveys conducted on October 18 and November 18, 2021 (Supp. Fig. S5). Thermal anomalies marking groundwater discharge were localized at depths of 2.4–2.6 m from the surface on the southwestern side and at depths of 3.2–3.4 m on the northwestern and southeastern sides of the lake basin. Apparently, water entered the basin through the contact of limestone and Quaternary sediments. During the survey of October 18, 2021, thermal anomalies on the water surface were also recorded, indicating subaqueous discharge of epikarstic waters (Fig. 3B, Supp. Fig. S5).

Some of the springs that opened in the basin (Nos. 1–5 in Fig. 3) discharged turbid water having a yellowish color, carrying iridescent films, and depositing ochre-colored, flaky precipitates of iron (oxy) hydroxides (Fig. 4). The smell of hydrogen sulfide was noted.

Evolution of Hydrochemistry During the Recovery of Lake Ygyshm

The waters filling the lake basin were characterized by HCO_3^-–Ca^{2+} composition, with other anions and cations (Cl^-, SO_4^{2-}, Mg^{2+}, $Na^+ + K^+$, NO_2^- and NO_3^-) present in minimal concentrations or not detected (Supp. Table S3). The total dissolved solids (TDS) of these waters are compared with other groups of natural waters in the Shulgan River basin in Fig. 5A. Most of the water has HCO_3^-–Ca^{2+} composition, indicating that dissolution of limestone is a primary process controlling water chemistry. The waters of the lakes (including Lake Ygyshma before the drainage event on September 28, 2021) were characterized by lower TDS (0.05–0.10 g L^{-1}) compared to karstic water and groundwater of Quaternary deposits (Fig. 5A, Supp. Table S3). This indicates predominantly atmospheric recharge of the lakes in their "normal" state.

At the beginning of Lake Ygyshma recovery (September 30, 2021), the TDS of water in the basin was 0.26 g L^{-1}, which significantly exceeded the mineralization of the lake water before its drainage. Subsequently, mineralization of lake water decreased in sync with the increase in water volume (Supp. Fig. S4), returning to pre-drainage values by June 2022. The waters of the eight springs that opened in the lake basin had TDS values of 0.12–0.30 g L^{-1}, which are consistent with groundwater and epikarstic water values (Fig. 5A).

For some springs, elevated concentrations of iron were observed (up to 2.5 mg L^{-1}). These springs opened during the first days of lake recovery (September 30 to October 10, 2021); concentration of iron in the lake water during that period of time increased from 0.25 to 0.50 mg L^{-1}. Subsequently, the iron content in the lake water decreased (Fig. 5B).

Vertical Gradient of Physical and Chemical Parameters of Water

To assess possible stratification of water temperature (T), electrical conductivity (EC), and pH, measurements were taken at various depths on June 23, 2022, in Lake Ollukul (Fig. 6). The measurements revealed a relatively uniform and low EC value (81–79 µS cm^{-1}) in the near-surface layer, to a depth of 1.2 m. Water temperature behaved in a more complex

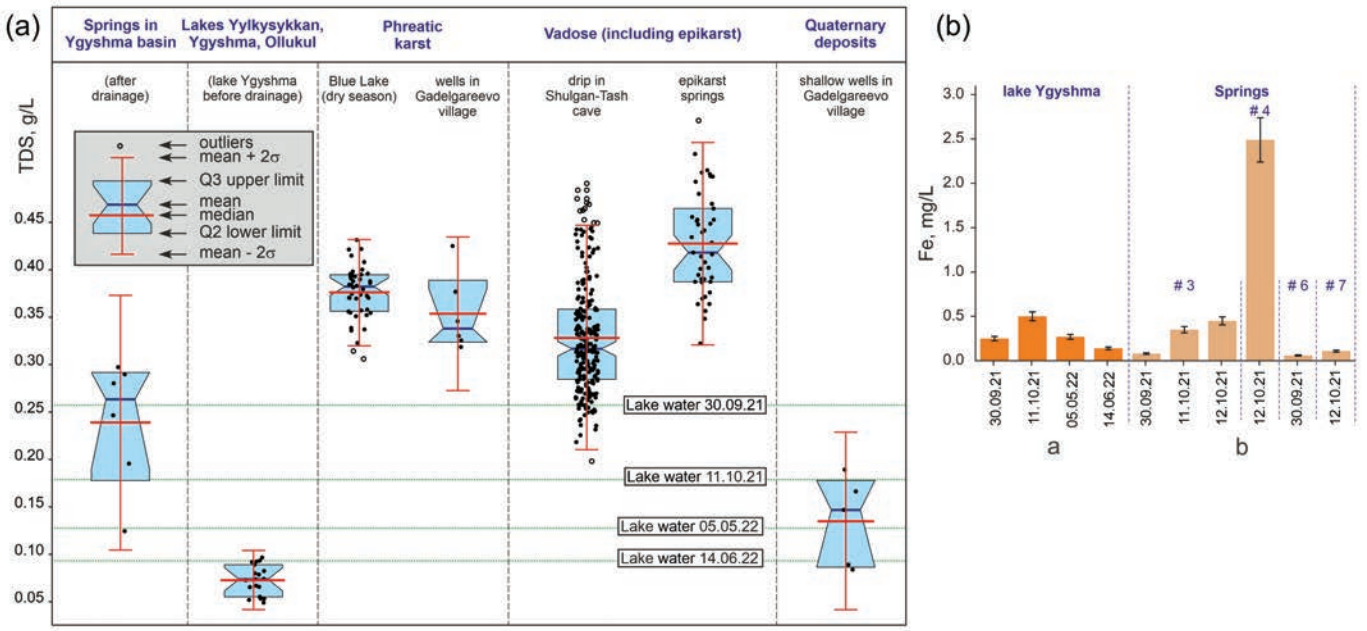

Figure 5. Comparison of selected chemical parameters of various waters from the study area. (A) Measurements (black dots) of the mineralization (TDS) of waters (*vertical axis*) from different types of sources (top row of purple column headings) and particular sources and times (second row of column headings) (cf. Supp. Table S3). Legend for statistical analysis shown in gray inset. Green horizontal lines represent the TDS of Lake Ygyshma over time as the lake recovered. (B) Iron content (vertical axis) and variation over time (columns) in selected waters of the study area. (*a*) Lake Ygyshma. (*b*) Selected numbered springs discharging into the basin Lake Ygyshma (as indicated in columns separated by dashed lines) (with error bars indicating analytical uncertainty of ±15 %)

way. Near the surface, within the first 0.3 m, T decreased sharply from 25.3 °C to 20.0 °C. This layer corresponds to the approximate penetration depth of the sun's rays. Water temperature was relatively stable (20.0 °C to 18.0 °C) between 0.3–1.2 m depth. Below the 1.2 m depth, T started to gradually decrease to reach 6.1 °C at 3.3 m. The EC increased in this depth interval from 80 to 138 µS cm^{-1}. More alkaline conditions (pH = 6.62–6.68) were observed in the surface and near-bottom layers. Between 0.3 and 1.4 m, lower pHs (6.13–6.20) were measured.

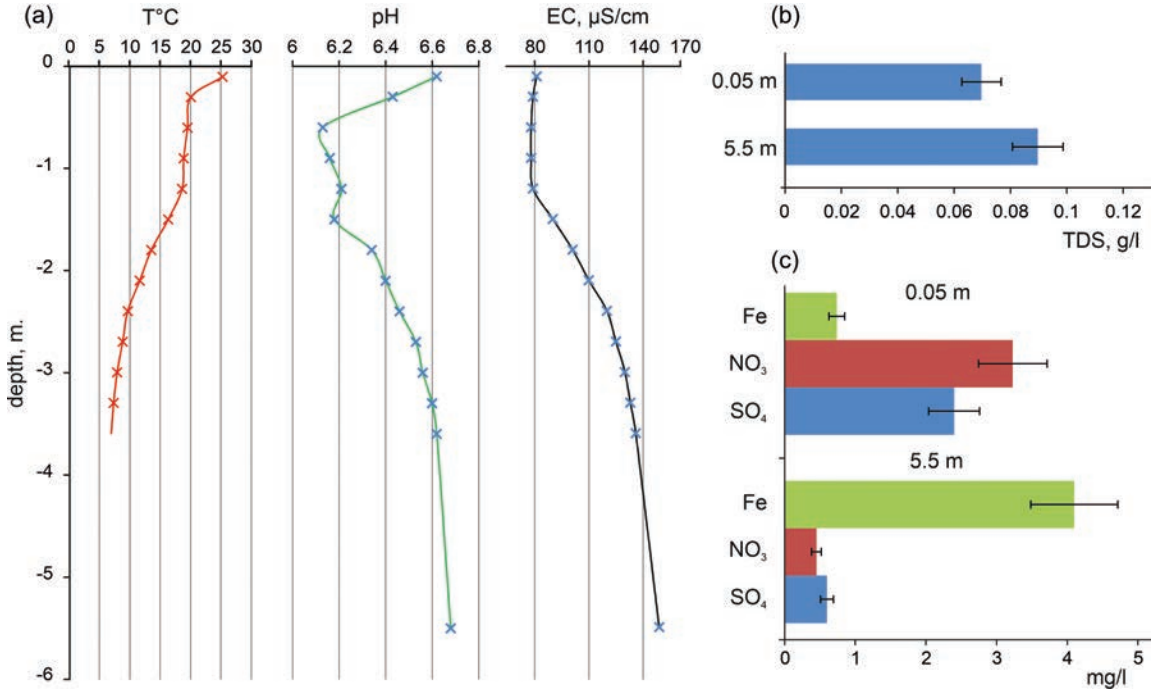

Figure 6. Charts of water parameters in Lake Ollukul: (A) Water temperature (T), pH, and electrical conductivity (EC) (horizontal axes) versus lake depth (vertical axis). (B) Mineralization (TDS) (horizontal axis) of water from the surface (depth = 0.05 m) and the lake bottom (depth = 5.5 m). (C) Concentrations of Fe, NO_3 and SO_4 (horizontal axis) of water from the surface (depth = 0.05 m) and the lake bottom (depth = 5.5 m).

Changes in water chemistry with lake depth are illustrated by two samples, one taken near the surface at a depth of 0.05 m and one at a depth of 5.5 m (Supp. Table S4). TDS slightly increased with depth from 0.07 to 0.09 g L^{-1} (Fig. 6B). The most contrasting behaviors were shown by the concentrations of oxidized compounds

(NO_3^- and SO_4^{2-}) and of iron: the concentrations of NO_3^- and SO_4^{2-} in the bottom layer decreased by factors of 7.2 and 4, respectively, and iron concentration increased by a factor of 5.5, reaching 4.1 mg L^{-1} (Fig. 6C).

Prerequisites for Authigenic Mineralization

The waters filling the Lake Ygyshma basin were undersaturated with respect to calcite (saturation index (SI) from –1.46 to –0.81) and siderite (SI from –1.18 to –0.67) under "closed-system" conditions. In calculations for "open-system" conditions, water of the lake in the early period of restoration (September 30, 2021 to October 11, 2021) showed supersaturation with respect to these carbonates (Supp. Table S5). Waters discharging from springs in the lake in closed-system conditions were mostly undersaturated with respect to calcite and siderite, but in open-system conditions, oversaturation reached SI = 0.91 for calcite and SI = 0.77 for siderite, which is consistent with precipitation of these minerals at the discharge point. The exception is weakly mineralized Spring No. 7 (Fig. 3) for which under-saturation was noted.

All waters were supersaturated with respect to iron (oxy) hydroxide, for Spring No. 6 only in open-system conditions and for the other springs in both open- and closed-system conditions. For the water of Lake Ygyshma, there was an increase in supersaturation from SI = 0.41 in October 2021 to SI = 2.68 in May 2022 (the closed-system calculation); this contributed to the precipitation of (oxy) hydroxides, and as a result, a decrease in the iron concentration in the water (Fig. 5*B*).

Mineral Deposits of Lake Ygyshma

Bottom sediments of the lake basin comprise inter-layers of coarse (5–30 mm) clastic material in fine-grained sapropelic sediments. This indicates periodic influxes of material with dynamic water flows. The main mineral in these clastic sediments is quartz (ca. 98 %). Potassic feldspars, which have undergone strong hydrolytic changes, comprise 1.0 % to 1.5 %. Among the accessory minerals, hematite, chromite, ilmenite, rutile, titanite, clinochlorite, garnet, and monazite were found (Supp. Materials). Some of these minerals (titanite and rutile) are characteristic of sandstones of the Takatinskaya Formation (Knyazev et al., 2015), which are the most probable source of clastic material in the lake basin.

Authigenic minerals in the sapropel sediments are not abundant (Fig. 7; Supp. Table S6). They are represented by lamellar microcrystals of rhodochrosite on quartz grains and granulomorphic siderite. Fibrous secretions of magnesium-bearing phyllosilicate, tentatively identified as saponite, were also found. Microgranules of authigenic barite were formed inside the matrix of organic polymers (Fig. 7D).

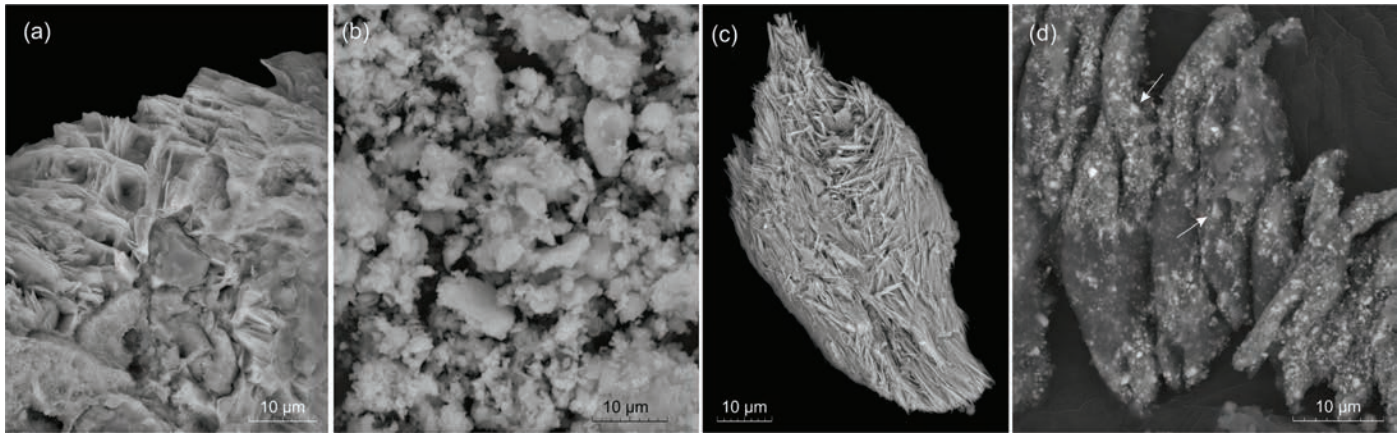

Figure 7. Scanning electron microscope images of authigenic minerals of lake sediments. (A) Rhodochrosite; (B) Siderite, (C) Magnesium-bearing phyllosilicate (possibly saponite), (D) Barite microgranules (arrows) embedded in a matrix of organic polymers.

Authigenic Mineralization and Development of Iron-Oxidizing Bacteria in Sediments of Discharging Springs

In the springs with ferruginous water that appeared in the lake basin, ochre deposits of iron (oxy) hydroxides were already visible in the first weeks. Finely-dispersed (oxy) hydroxides also formed adhesive aggregates, sometimes with nodule-like textures (Fig. 8A). The SEM-EDS analysis of these deposits revealed their microglobular structure with individual globules as small as 0.5 µm (Fig. 8B). The high carbon content of these globules (ca. 24 % by mass) suggests their association with organic colloids, presumably fulvic acids. Microbial structures with stem-like morphologies (Fig. 8C) and with tubular sheaths 0.2–0.4 µm thick with bud-like fouling of iron (oxy) hydroxides are common (Fig. 8D–E). Such structures are characteristic of neutrophilic, chemoautotrophic aerobic, and microaerophilic iron-oxidizing bacteria. The sheath-shaped structures correspond to *Leptothrix* spp., most probably *L. ochracea*, and the type with stem morphology correspond to *Gallionella* spp. (Katsoyiannis and Zouboulis, 2004; Hallbeck et al., 2005; Johnson et al., 2012; Spring and Kämpfer, 2005; Fleming et al., 2014).

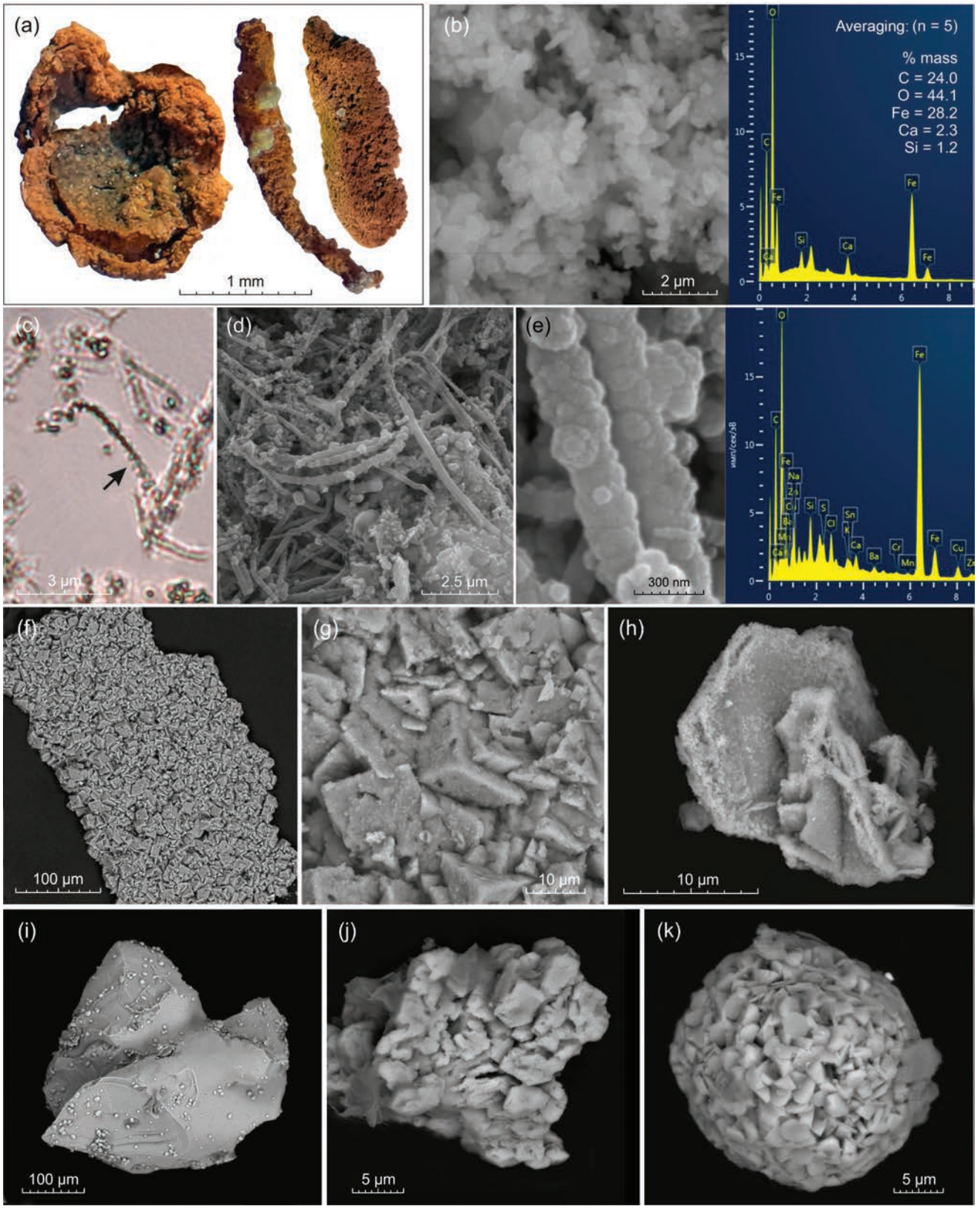

Figure 8. Composite macrophotography (A), scanning electron microscope (SEM) images (B, D–K), and light-field optical photomicrograph (*C*) of authigenic minerals forming at spring orifices in the Lake Ygyshma basin. (A) Nodular aggregates of iron (oxy) hydroxides. (B) Globular microstructure of iron (oxy) hydroxides deposited on organic colloids and their typical energy-dispersive X-ray spectroscopy (EDS) spectrum. (C) Microbial filaments associated with iron-oxidizing bacteria, and spiral stalks (*black arrow*) characteristic of *Gallionella* spp. (D) Long filamentous mineral sheaths characteristic of *Leptothrix* spp. (E) Details of the structure of the mineral sheaths of *Leptothrix* spp., and typical EDS spectrum of mineral sheaths. (F) Raft-like calcite aggregates. (G) Details of structure of newly formed calcite. (H) Siderite crystals. (I) Amorphous precipitates of aluminosilicates. (J) Barite aggregate. (K) Framboidal pyrite.

In addition to iron (oxy) hydroxides, several other authigenic minerals were found in the spring precipitates (see Supp. Fig. S6 for their EDS spectra). The most common minerals are calcite composed of intergrown rhombohedral crystals (Fig. 8F–G) and siderite represented by lamellar crystals 10–15 μm in size (Fig. 8H). Collomorphic clumps of authigenic phyllosilicates up to 800 μm in size were observed (Fig. 8I). Microcrystals and aggregates of barite up to 60 μm in size were also found (Fig. 8J) formed in media rich in organic polymers. The presence of framboidal pyrite (Fig. 8K) indicates sulfate-reduction processes and the presence of bisulfide and hydrogen sulfide in the spring water. In addition, minor occurrences of gypsum were found, suggestive of sulfide oxidation (Supp. Fig. S6).

DISCUSSION

Karstic Lakes of the Shulgan River Valley

There are five permanent karstic lakes in the Shulgan River basin (more specifically, in the dry Shulgan Valley), two of which have been converted into peat bogs. All lakes are confined to deep karstic depressions. Based on the classification of karstic lakes by Kindinger et al. (1999), Lakes Ollukul, Fatima, and Dvoinoye belong to the mature base-level-phase type of lakes that have completely lost their connection with karstic channels. Lakes Yylkysykkan and Ygyshma belong to the transit type, for which communication with karstic channels is difficult, but possible in certain periods of time.

Degradation of Karstic Lakes of the Shulgan Valley and Transformation of Hydrochemical Conditions in Them

Lakes in the waterless Shulgan Valley are subject to terrestrialization (the term defines a succession whereby a pond or a lake fills with sediments and peat over an extended period of time (Craft, 2016)). The observed state of karstic lakes known as “karstic bogs” is well studied in the European part of Russia, as well as in the pre-Urals (Volkova, 2010; Baisheva et al., 2012; Tsyganov et al, 2019). Swamping begins with the development of peat rafts that gradually close the surface of the water body. The initial formation of the floating mats (splavinas) is due to leaf litter; then green mosses and pioneer vegetation populate the substratum. Over time, the splavinas turn into floating “islands” populated by shrubs and trees, dominated by birch, which is more resistant to nutrient deficiency. As the thickness of the floating mats increases further, it loses tree and shrub vegetation and becomes populated by mosses. Water is preserved under the floating peat layer, which gradually covers the entire pond surface.

The degradation of karstic lakes in the Shulgan Valley accelerated in the second half of the twentieth century: since 1959, two of the five lakes have ceased to exist as lakes, having been converted to peat bogs. Presumably, anthropogenic processes, such as change of natural flow during construction of the highway and pollution of lakes with timber, played a role in this conversion.

Data from Lake Ollukul show significant enrichment of the bottom water with iron (up to 4.1 mg L^{-1}). This indicates anaerobic reducing conditions in which iron is subjected to microbial reduction and is in the form of Fe^{2+} (Lovley et al., 1990). The source of Fe^{2+}/Fe^{3+} is most likely related to the incongruent dissolution of feldspars, which contain iron as an impurity (see Supp. Materials). Another noteworthy feature is the absence of oxidized compounds SO_4^{2-} and NO_3^- in the bottom water, presumably due to anaerobic microbial processes: denitrification and sulfate reduction. The near-surface layer of the lake water has relatively low pH, which may indicate bacterial oxidation of gases (hydrogen sulfide, methane) when they ascend into the oxidative zone. The observations show that in the hypolimnion zone of karstic lakes, reducing conditions are formed in which, under the influence of microbial-conditioned geochemical processes, the water composition acquires properties typical of suboxic bog water (Guseva, 2016).

Mechanism of Rapid Drainage of Lake Ygyshma

The rapid drainage of the Lake Ygyshma on the night of September 27 to 28, 2021 implies that there is, potentially, a good hydraulic connection between the lake and the underground karstic channels of the phreatic zone. In normal conditions, this connection is choked by lake bottom sediments. Disruption of the “plug” led to a precipitous drainage of the lake into the phreatic zone. The related spike on the hydrographs recorded at two stations in the Shulgan-Tash Cave had a single-peak shape, and showed no recession limb, indicating that flow was via channel conduits.

All three known episodes of rapid drainage of Lake Ygyshma (in 1921, 1978, and 2021) occurred during severe summer droughts. Apparently, under the ordinary hydrological regime, the sediment plug is kept buoyant by the phreatic waters. During droughts, the level of phreatic water decreases, the buoyant support diminishes, and the plug can be broken due to pressure exerted by the mass of lake water.

Recovery of Lake Ygyshma and Overflow of Water from Lake Dvoinoye

Monitoring of the lake recovery rate and its water chemistry from September 2021 to June 2022 showed that the increase of water volume and concomitant decrease of TDS are well approximated by a logarithmic function (R^2 = 0.96 and 0.95, respectively). Consequently, the water inflow into the lake followed the exponential law. This pattern of inflow recession indicates involvement of multiple elements of the massif void space (Atkinson, 1977; White, 1988; Ford and

Williams, 1989; Fiorillo, 2014). Waters of epikarst (a zone characterized by high permeability and rate of yield as well as elevated TDS) were involved at the initial stages of lake recovery, while groundwater from Quaternary sediments (lower permeability and rate of yield and lower TDS) became more important at the later stages.

Among the springs opened on the sides of the dried lake basin (Fig. 3), two types can be distinguished: (1) springs with relatively low TDS and low content of iron (Spring Nos. 6, 7, and 3 in the first days after emergence) and (2) springs with higher TDS and elevated iron content (Spring Nos. 4 and 3 in the later stages). In addition to the elevated iron contents (up to 2.5 mg L^{-1}) and the absence of NO_3^- and SO_4^{2-}, the waters of the latter two springs had an odor of hydrogen sulfide and contained organic colloids. This set of characteristics indicates the formation of water under anoxic reducing conditions (similar to those observed at the bottom of Lake Ollukul). Springs discharging water of this type appeared in the southwestern and western sides of the Lake Ygyshma basin. We interpret this as indication of flow from the Lake Dvoinoe, located 48 m upstream the Shulgan Valley (Fig. 9A). Apparently, the sudden draining of water from Lake Ygyshma formed a depression funnel and caused the flow of water, preserved under the peat bog cover of Lake Dvoynoe along the contact between Quaternary sediments and limestone (Fig. 9B).

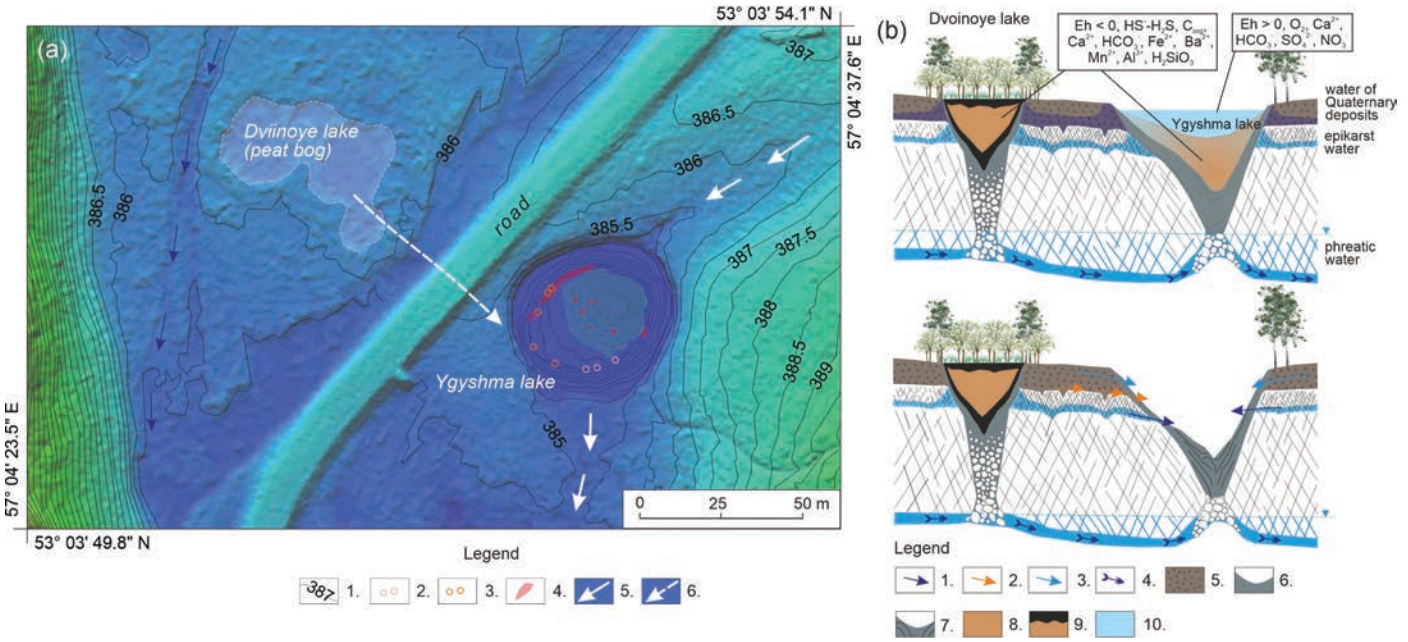

Figure 9. Illustrations of the flow of water from the peat bog Lake Dvoinoe to Lake Ygyshma after rapid draining of the latter. (A) Map of the Lakes Ygyshma and Dvoinoe basin based on the digital relief model by Svoyskiy et al. (2020) and the authors' data. Legend: (1) Elevation contours in m a.s.l. (Baltic system of elevation). (2) Springs discharging low-TDS water. (3) Springs discharging iron-enriched water. precipitating iron (oxy) hydroxides, and developing of iron-oxidizing bacteria. (4) Main thermal anomalies. (5) Direction of surface flow. (6) Inferred direction of groundwater flow.

(B) Idealized cross section of Lakes Dvoinoe and Ygyshma illustrating the hydrogeological situation before and after drainage of the latter. Drainage is caused by disruption of sediment plug at the bottom of the lake, and conditions for recovery arise when the plug is restored by landslide processes. Legend: (1) Epikarstic water. (2) Water of Lake Dvoinoe. (3) Groundwater of Quaternary deposits. (4) Phreatic water. (5) Quaternary deposits (gravely and sandy silts of Middle Pleistocene to Holocene age). (6) Intact lake sediments. (7) Lake sediments displaced by landslides. (8) Reducing lake water. (9) Peat deposits and sub-peat water. (10) Oxidizing lake water.

Geochemical and Mineralogenic Processes Associated with the Restoration of Lake Ygyshma

Suboxic lake waters, represented by hypolimnionic waters of open lakes of the Shulgan Valley and sublacustrine waters of Lake Dvoinoye (which flowed into Lake Ygyshma), have high concentrations of iron (up to 4.1 mg L^{-1}). The latter may be sourced by incongruent dissolution of feldspars (see Supp. Materials 2). Organic carbon is used by ferrous- (Fe^{2+}), ferric- (Fe^{3+}), and sulfate- (SO_4^{2-}) reducers as an electron donor and carbon source (Roh et al., 2003), resulting in a system enriched of carbonic acid, which further enhances incongruent dissolution of silicates. This hypothetical process also explains the presence of typical hydrolysates (Al^{3+}, H_2SiO_3, Mn^{2+}) involved in authigenic mineral formation (as impurities, and as independent phases: phyllosilicates and rhodochrosite). In addition, this mechanism could be responsible for the appearance of bicarbonate ions in the water, which enables precipitation of carbonates.

At the outlet of reducing bog water into the oxidative zone in the springs in the Lake Ygyshma basin, a redox barrier is formed, on which $Fe^{2+} \rightarrow Fe^{3+}$ oxidation and precipitation of iron (oxy) hydroxides occurs. Observations show that iron (oxy) hydroxides were transferred and precipitated on colloids of organic matter, presumably fulvic acids. Fulvic and humic acids are known to be strong complexing agents, promoting transport and accumulation of metals (Furukawa and

Takahashi, 2008). The associated iron-aluminum-organic colloids carrying absorbed metals can be stable in bog water for long periods of time (Pokrovsky et al., 2005). The redox barrier at spring discharge points also promoted activity of iron-oxidizing bacteria. The latter were identified by the sheath morphology as *Leptothrix ochracea* and *Gallionella* spp. The environment in which iron-oxidizing bacteria develop is known to be characterized by a high concentration of dissolved Fe^{2+}, low pO_2, and near-neutral pH (Johnson et al., 2012; Emerson and Revsbech, 1994; Fleming et al., 2014; Lin et al., 2012; Stein et al., 2001).

When entering the oxidation zone, the waters of Lake/bog Dvoinoye are supersaturated with respect to calcite and siderite (due to the difference in pCO_2 in water and air; Supp. Table S4). Both carbonates were found in authigenic spring sediments. Interestingly, siderite was also identified in the bottom sediments of Lake Ygyshma, which does not agree with the closed-system model estimates. It is possible that in sapropel lake sediments, carbonate deposition is controlled by microbially mediated processes, such as nitrogen respiration and anaerobic sulfate reductions (Machel, 2001; Castanier et al., 2010).

The presence of framboidal pyrite sources in sediments, as well as the hydrogen sulfide odor, are indicative of the reducing, oxygen-free conditions and the development of sulfate-reducing bacteria. Growth of framboidal pyrite occurs by an explosive nucleation mechanism, with reactions between FeS and polysulfide particles or hydrogen sulfide and a pH over 5, often in association with organic material (Rickard, 2021).

Sulfate mineral formation (barite and gypsum) has been noted in spring sediments. Barite has been found exclusively in samples rich in organics (in association with organic polymers). There is increasing evidence that microbial activity may contribute to barite precipitation (Stevens et al., 2015; Senko et al., 2004; Dehairs et al., 2008). The appearance of gypsum may be due to oxidation of sulfides with further reaction of sulfuric acid with carbonates.

Implications of Lake Ygyshma Drainage for Understanding the Mineralogy of Shulgan-Tash Cave

Shulgan-Tash is a large cave, featuring a variety of common, mostly calcite speleothems, such as stalagmites and flowstone. In addition, speleothems composed of other minerals have been reported from the cave walls, for example (oxy) hydroxides (Lyakhnitsky et al., 2013) and sulfates (Chervyatsova et al., 2018). Cryogenic cave calcite of Pleistocene age was reported from cave sediments (Dublyansky et al., 2018). Large (up to several centimeters) crystals of cryogenic gypsum have been found in the cave, and barite, rhodochrosite, and siderite are minor minerals in the cryogenic minerals. The presence of such minerals suggests that mineral-forming waters may have chemical properties distinct form typical low-TDS, carbonate karstic waters.

As discussed above, the waters of karstic lakes in the Shulgan Valley have contrasting characteristics. The surface layers of open, drainless lakes (open-water surfaces, e.g., Lake Ygyshma) are characterized by oxygen-oxidative conditions. They typically have relatively low mineralization (TDS = 0.05–0.1 g L^{-1}) and contain oxidized compounds (SO_4^{2-}, NO_3^-). In terrestrialized eutrophic lakes (e.g. Lake Dvoinoye) and in hypolimnionic zones of open lakes, a reducing geochemical setting locally develops. Waters of such reservoirs are enriched with organic colloids and hydrolysates and may contain hydrogen sulfide and other gases.

If the integrity of bottom sediments plugging the connection between an isolated karstic lake basin and the underlying karstic conduits is broken, the lake waters flow into the underlying karstic cavities. In modern climatic and hydrogeological conditions, such waters enter the rather powerful stream of karstic waters flowing through the phreatic zone of the Shulgan-Tash System. As a result, these waters are diluted and pass through the karstic system as a short, barely-noticeable pulse. Regardless of their chemical composition (reducing water of peat bog lakes or oxygenated water of open lakes), the waters have no significant impact on the underground environment and leave no geochemical or mineralogical traces in the karstic conduits through which they pass.

However, in the climatic conditions of the Pleistocene, drainage of lakes may have had much more significant consequences. Between ca. 60,000 and 14,000 YBP, the Shulgan-Tash area was affected by permafrost. During the moderately cold stage of MIS 3, the upper boundary of the permafrost repeatedly moved up and down in the rock massifs hosting caves (Dublyansky et al., 2018). During periods of permafrost aggradation, the inflow of precipitation into underground karstic channels was hindered, leading to the formation of waterlogged, supra-permafrost reservoirs in karstic sinkholes. When the permafrost degraded and its upper boundary lowered, pulse-like inflow of significant volumes of bog water into the karstic cavities could have taken place. Such episodic inflows could be responsible for deposition of (small amounts of) minerals not typical of the epigenetic carbonate karst.

CONCLUSIONS

All five lakes known in the Shulgan River basin are restricted to deep karstic depressions, the maximum depths of which approach the level of karstic aquifer. The lakes are isolated from the underlying karstic channels by plugs of bottom sediments; they are primarily fed by precipitation. They are affected in varying degrees by terrestrialization and eutrophication processes; two lakes are presently at the stage of peat bog. In the future, the structure of lake basins and the thickness of bottom sediments should be clarified by geophysical methods.

In degrading lakes, local reducing conditions are developed and corresponding geo- and biochemical processes take place (hydrolysis of silicates, accumulation of transit metals, sulfate reductions, nitrogen respiration, and sulfide deposition). Geomicrobiological studies of lake sediment water are needed to reveal the biogeochemical mechanisms in more detail.

In lake Ygyshma, episodes of rapid drainage occur approximately once every 50 years. During the last episode, in September 2021, we were able to observe that the lake waters pass through the karstic channels and are discharged from a spring located 2.8 km down the valley. The escape of water from the lake created a depression funnel, which caused the flow of reducing anoxic water from the neighboring Lake/bog Dvoinoye. As this water entered the oxidative zone, the iron (oxy) hydroxides, calcite, siderite, authigenic aluminosilicates, barite, pyrite, and gypsum were deposited on the redox barrier, and communities of iron-oxidizing bacteria were developing.

ACKNOWLEDGMENTS

The authors are grateful to I.I. Musabirov (Institute for Metals Superplasticity Problems, Russian Academy of Sciences, Ufa, Russia) for support with SEM and EDS analyses; N.M. Sayfullina and M.N. Kosarev (Shulgan-Tash Nature Reserve, Irgizly Village, Bashkortostan, Russia) for consultations; and Y.S. Lyakhnitsky (A.P. Karpinsky Russian Geological Research Institute, St. Petersburg, Russia) for providing archive materials of aerial survey and participation in discussion. We are also grateful to two anonymous reviewers for valuable comments that greatly improved the manuscript.

Olga Chervyatsova's work was performed within the state assignment of the Russian Ministry of Ecology and Natural Resources No. 2-22-91-2 on topic no. 122092200006-4. Ludmila Kuzmina's work was carried out within the framework of the state assignment of the Ministry of Education and Science of Russia No. 075-03-2021-607 on the topic no. 122031100163-4 with the use of equipment of the Ufa Federal Research Center of the Russian Academy of Sciences "Agidel" Center for Collective Use.

REFERENCES

Abdrakhmanov, R.F., Popov, V.G., Rozhdestvensky, A.P., Smirnov, A.I., and Travkin, A.I., 2002, Karst Bashkortostana (Karst of Bashkortostan), Ufa, Bashkortostan Republic, Russia, Informreklama, 382 p., http://ig.ufaras.ru/File/PubTxt/ABDR/Karst.pdf.

Andrić, I., and Bonacci, O., 2014, Morphological study of Red Lake in Dinaric karst based on terrestrial laser scanning and sonar systems: Acta Carsologica, v. 43, p. 229–239, https://doi.org/10.3986/ac.v43i2.712.

Atkinson, T.C., 1977, Diffuse flow and conduit flow in limestone terrain in the Mendip Hills, Somerset (Great Britain): *Journal of Hydrology*, v. 35, p. 93–100, https://doi.org/10.1016/0022-1694(77)90079-8.

Baisheva, E.Z., Muldashev, A.A., Martynenko, V.B., Minaeva, T.Y., and Shirokikh, P.S., 2012, Flora karstovykh bolot Bashkirskogo Preduralya [Flora of karst bogs of the Bashkirian Pre-Urals]: Botanicheskiĭ Zhurnal, v. 97, p. 1010–1039, https://doi.org/10.1134/S1234567812080022.

Bonacci, O., Andrić, I., and Yamashiki, Y., 2014, Hydrology of Blue Lake in the Dinaric karst: Hydrological Processes, v. 28, p. 1890–1898, https://doi.org/10.1002/hyp.9736.

Bücker, M., et al., 2021. Integrated land and water-borne geophysical surveys shed light on the sudden drying of large karst lakes in southern Mexico: Solid Earth, v. 12, p. 439–461, https://doi.org/10.5194/se-12-439-2021.

Castanier, S., Le Métayer-Levrel, G., and Perthuisot, J.-P., 2000, Bacterial roles in the precipitation of carbonate minerals, *in* Riding, R.E., and Awramik, S.M., eds., Microbial Sediments, Berlin, Springer-Verlag, p. 32–39, https://doi.org/10.1007/978-3-662-04036-2_5.

Chervyatsova O.Ya., Lyakhnitskiy, Yu.S., and Gaynutdinov, I.A., 2015, The Shulgan River and Shulgan-Tash Cave (the southern Urals) spring flood features, *in* Speleology and Speleostology: Proceedings of the VI International Scientific Correspondence Conference, Nabereznye Chelny, Tartarstan, Russia, p. 87–97, https://pro-speleo.ru/Conf2015/SiS-2015.pdf.

Chervyatsova, O.Y., Potapov, S.S., Sadykov, S.A., Dublianskii, I.V., Musabirov, I.I., and Demeni, A., 2018, K voprosu o genezise subaeral-nykh otlozhenii gipsa v Peshchere Shulgan-Tash [On the genesis of subaerial gypsum deposits in the Shulgan-Tash Cave]: Izvestiya Ufimskogo Nauchnogo Tsentra RAN, v. 1, p. 58–65, https://doi.org/10.31040/2222-8349-2018-0-1-58-65.

Craft, C., 2016, Creating and Restoring Wetlands: From Theory to Practice, Amsterdam, Elsevier, 348 p., https://doi.org/10.1016/B978-0-12-407232-9.01001-0.

Dehairs, F., et al., 2008, Barium in twilight zone suspended matter as a potential proxy for particulate organic carbon remineralization: Results for the North Pacific: Deep-Sea Research II, v. 55, p. 1673–1683, https://doi.org/10.1016/j.dsr2.2008.04.020.

Dublyansky, Y., Moseley, G.E., Lyakhnitsky, Y., Cheng, H., Edwards, L.R., Scholz, D., Koltai, G., and Spötl, C., 2018, Late Palaeolithic cave art and permafrost in the Southern Ural: Scientific Reports, v. 8, p. 12080, https://doi.org/10.1038/s41598-018-30049-w.

Emerson, D., and Revsbech, N.P., 1994, Investigation of an iron-oxidizing microbial mat community located near Aarhus, Denmark: Field studies: Applied and Environmental Microbiology, v. 60, p. 4022–4031, https://doi.org/10.1128/aem.60.11.4022-4031.1994.

Fiorillo, F., 2014, The recession of spring hydrographs, focused on karst aquifers: Water Resources Management, v. 28, p. 1781–1805, https://doi.org/10.1007/s11269-014-0597-z.

Fleming, E.J., Cetinić, I., Chan, C.S., King, D.W., and Emerson, D., 2014, Ecological succession among iron-oxidizing bacteria: ISME Journal, v. 8, p. 804–815, https://doi.org/10.1038/ismej.2013.197.

Ford, D.C., and Williams, P.W., 1989, Karst Geomorphology and Hydrology, London, Unwin Hyman, 601 p.

Furukawa, K., and Takahashi, Y., 2008, Effect of complexation with humic substances on diffusion of metal ions in water: Chemosphere, v. 73, p. 1272–1278, https://doi.org/10.1016/j.chemosphere.2008.07.017.

Guseva, N., 2016, The origin of the natural water chemical composition in the permafrost region of the eastern slope of the Polar Urals: Water, v. 8, p. 594, https://doi.org/10.3390/w8120594.

Hallbeck, L.E-L., and Pedersen, K., 2005, Genus I: *Gallionella* Ehrenberg 1838, *in* Brenner, D.J., Krieg, N.R., and Staley, J.T., eds., Bergey's Manual of Systematic Bacteriology, New York, Springer, 2nd ed., v. 2, part C, pp. 880–886, https://doi.org/10.1002/9781118960608.gbm00988.

Hammer, Ø., Harper, D.A.T., and Ryan, P.D., 2001, PAST: Paleontological statistics software package for education and data analysis: Palaeontologia electronica, v. 4, 9 p., https://palaeo-electronica.org/2001_1/past/past.pdf.

Johnson, K.W., Carmichael, M.J., McDonald, W., Rose, N., Pitchford, J., Windelspecht, M., Karatan, E., and Bräuer, S.L., 2012, Increased abundance of *Gallionella* spp., *Leptothrix* spp. and total bacteria in response to enhanced Mn and Fe concentrations in a disturbed Southern Appalachian high elevation wetland: Geomicrobiology Journal, v. 29, p. 124–138, https://doi.org.10.1080/01490451.2011.558557.

Katsoyiannis, I.A., and Zouboulis, A.I., 2004, Application of biological processes for the removal of arsenic from groundwaters: Water Research, v. 38, p. 17–26, https://doi.org/10.1016/j.watres.2003.09.011.

Kindinger, J.L., Davis, J.B., and Flocks, J.G., 1999, Geology and evolution of lakes in north-central Florida: Environmental Geology, v. 38, p. 301–321, https://doi.org/10.1007/s002540050428.

Knyazev, Y.G., Knyazeva O.U., and Karimov T.R., 2015, Gosudarstvennaya Geologicheskaya Karta Rossiiskoi Federatsii, Seria Yuzhno-Uralskaya [State Geological Map of the Russian Federation, South Uralskaya Series], Moscow Branch of the All-Russian Scientific Research Geological Institute, scale 1:200,000, sheet N-40-XXVIII, second edition, explanatory note, VSEGEI, 237 p., http://geo.mfvsegei.ru/200k/Zap/Zap_N-40-XXVIII.pdf.

Kudryashov, I.K., 1969, Putevoditel po Kapovoi Peshchere [Guide to the Kapova Cave], Ufa, Bashkortostan Republic, Russia, Bashkirskoe Book Publishing House, 126 p.

Kuzmina, L.Y., Ryabova, A.S., Chervyatsova O.Ya., and Lyakhnitsky Y.S., 2013, Ocenka sanitarno-mikrobiologicheskogo i gidrohimicheskogo sostojania vodotokov zapovednika Shulgan-Tash [Evaluation of sanitary-microbiological and hydrochemical condition of water flows of the Shulgan-Tash Reserve]: Izvestia Samarskogo Nauchnogo Centra RAN [News of Samara Scientific Centre of the RAS], v. 15, p. 1329-1333, http://www.ssc.smr.ru/media/journals/izvestia/2013/2013_3_1329_1333.pdf.

Leal-Bautista, R.M., Perry, E.C., Alvarado-Flores, J., Alzate-Gavira, L., Domínguez-Maldonado, J.A., and Tapia-Tussell, R., 2021, Karst drainage of Lake Chakanbacán and its relation to Icaiche Formation: Boletín de la Sociedad Geológica Mexicana, v. 73, p. A021020, https://doi.org/10.18268/BSGM2021v73n1a021020.

Lin, C., Larsen, E.I., Nothdurft, L.D., and Smith, J.J., 2012, Neutrophilic, microaerophilic Fe(II)-oxidizing bacteria are ubiquitous in aquatic habitats of a subtropical Australian coastal catchment: Ubiquitous FeOB in catchment aquatic habitats: Geomicrobiology Journal, v. 29, p. 76–87, https://doi.org/10.1080/01490451.2010.523446.

Lovley, D.R., Chapelle, F.H., and Phillips, E.J.P., 1990, Fe(III)-reducing bacteria in deeply buried sediments of the Atlantic Coastal Plain: Geology, v. 18, p. 954–957, https://doi.org/10.1130/0091-7613(1990)018<0954:FIRBID>2.3.CO;2.

Lyakhnitsky Y.S., and Shchelinsky V.E., 1987, Issledovaniya Kapovoy Peshchery (Shulgan-Tash) [Research of the Kapova Cave (Shulgan-Tash)]: Izvestiya Vsesoyuznogo Geograficheskogo Obshchestva [Bulletin of the All-Union Geographical Society], v. 119, p. 548–553, https://elib.rgo.ru/handle/123456789/219030.

Lyakhnitsky Y.S., and Chuiko M.A. 2001. Kompleksnyye yestestvenno-nauchnyye issledovaniya Kapovoy Peshchery (Shulgan-Tash) kak osnova Spaseniya yeye Paleoliticheskoy Zhivopisi [Complex natural-scientific research of the Kapova Cave (Shulgan-Tash) as a basis for saving its Paleolithic painting], *in* Problemy Pervobytnoy Kultury [Problems of Primitive Culture], Ufa, Bashkortostan Republic, Russia: Gilem Publishing House, p. 190-212, https://www.old.archeo.ru/izdaniya-1/vagnejshije-izdanija/pdf/2001Problemy_Pervob_Kult.pdf/view?_x_tr_sl=auto&_x_tr_tl=en&_x_tr_hl=en-US&_x_tr_pto=wapp.

Lyakhnitsky, Y.S., Minnikov, O.A., and Yushko, A.A., 2013, Risunki i Znaki Peshchery Shulgan-Tash (Kapovoi): Katalog Izobrazhenii [Drawings and Signs of Shulgan-Tash (Kapova) Cave: Catalogue of Images], Ufa, Bashkortostan Republic, Russia, Kitap, 286 p., https://www.rgo.ru/sites/default/files/kniga_kapova_peshchera_.pdf.

Machel, H.G., 2001, Bacterial and thermochemical sulfate reduction in diagenetic settings: Old and new insights: Sedimentary Geology, v. 140, p. 143–175, https://doi.org/10.1016/S0037-0738(00)00176-7.

Mayaud, C., Gabrovšek, F., Blatnik, M., Kogovšek, B., Petrič, M., and Ravbar, N., 2019, Understanding flooding in poljes: A modelling perspective: Journal of Hydrology, v. 575, p. 874–889, https://doi.org/10.1016/j.jhydrol.2019.04.092.

Mayaud, C., Kogovšek, B., Gabrovšek, F., Blatnik, M., Petrič, M., and Ravbar, N., 2022, Deciphering the water balance of poljes: Example of Planinsko Polje (Slovenia): Acta Carsologica, v. 51, p. 155–157, https://doi.org/10.3986/ac.v51i2.11029.

McCormack, T., O'Connell, Y., Daly, E., Gil, L.W., Henry, T., and Perriquet, M., 2017, Characterisation of karst hydrogeology in Western Ireland using geophysical and hydraulic modelling techniques: Journal of Hydrology: Regional Studies, v. 10, p. 1–17, https://doi.org/10.1016/j.ejrh.2016.12.083.

Nazarova, A.A., and Boeva, L.V., 2002, Metodicheskie Ukazaniia Raschet Obshchego Soderzhaniia Natriia i Kaliia i Obshchego go Soderzhaniia Ionov v Poverkhnostnykh Vodakh Sushi [Calculation of the total sodium and potassium content and total ion content in inland surface waters], Rostov-on-Don, Rostov Oblast, Russia, Gidrokhimicheskim Institutom, https://meganorm.ru/Data2/1/4293829/4293829642.htm.

Pokrovsky, O.S., Dupré, B., and Schott, J., 2005, Fe–Al–organic colloids' control of trace elements in peat soil solutions: Results of ultrafiltration and dialysis: Aquatic Geochemistry, v. 11, p. 241–278, https://doi.org/10.1007/s10498-004-4765-2.

Ravbar, N., Mayaud, C., Blatnik, M., and Petrič, M., 2021, Determination of inundation areas within karst poljes and intermittent lakes for the purposes of ephemeral flood mapping: Hydrogeology Journal, v. 29, p. 213–228, https://doi.org/10.1007/s10040-020-02268-x.

Rickard, D., 2021, Framboids, New York, Oxford University Press, 334 p., https://doi.org/10.1093/oso/9780190080112.001.0001.

Roh, Y., Zhang, C.-L., Vali, H., Lauf, R.J., Zhou, J., and Phelps, T.J., 2003, Biogeochemical and environmental factors in Fe biomineralization: Magnetite and siderite formation: Clays and Clay Minerals, v. 51, p. 83–95, https://doi.org/10.1346/CCMN.2003.510110.

Roningen, J.M., and Burbey, T.J., 2012, Hydrogeologic controls on lake level: A case study at Mountain Lake, Virginia, USA, Hydrogeology Journal, v. 20, p. 1149–1167, https://doi.org/10.1007/s10040-012-0859-x.

Senko, J.M., Campbell, B.S., Henriksen, J.R., Elshahed, M.S., Dewers, T.A., and Krumholz, L.R., 2004, Barite deposition resulting from phototrophic sulfide-oxidizing bacterial activity: Geochimica et Cosmochimica Acta, v. 68, p. 773–780, https://doi.org/10.1016/j.gca.2003.07.008.

Shulgan-Tash Cave Museum-Reserve, 2020, unpublished historical and cultural digital archive.

Shulgan-Tash State Natural Biosphere Reserve, 1985–2016, Letopis prirody [Chronicle of Nature] (unpublished).

Sironić, A., Barešić, J., Horvatinčić, N., Brozinčević, A., Vurnek, M., and Kapelj, S., 2017, Changes in the geochemical parameters of karst lakes over the past three decades: The case of Plitvice Lakes, Croatia, Applied Geochemistry, v. 78, p. 12–22, https://doi.org/10.1016/j.apgeochem.2016.11.013.

Spring, S., and Kämpfer, P., 2005, Genus Incertae Sedis XIII: *Leptothrix* Kützing 1843 *in* Brenner, D.J., Krieg, N.R., and Staley, J.T., eds., Bergey's Manual of Systematic Bacteriology, New York, Springer, 2nd ed., v. 2, part C, pp. 740–746, https://doi.org/10.1002/9781118960608.gbm00955.

Stein, L.Y., La Duc, M.T., Grundi, T.J., and Nealson, K.H., 2001, Bacterial and archaeal populations associated with freshwater ferromanganous micronodules and sediments: Environmental Microbiology, v. 3, p. 10–18, https://doi.org/10.1046/j.1462-2920.2001.00154.x.

Stevens, E.W.N., Bailey, J.V., Flood, B.E., Jones, D.S., Gilhooly, W.P., III, Joye, S.B., Teske, A., and Mason, O.U., 2015, Barite encrustation of benthic sulfur-oxidizing bacteria at a marine cold seep, Geobiology, v. 13, p. 588–603, https://doi.org/10.1111/gbi.12154.

Svoyskiy, Yu.M., Romanenko, E.V., Grigoryev, N.N., and Levanova, E.S., 2020, Opyt dokumentirovaniia Peshchery Shulgan-Tash (Kapovoi) i okruzhaiushchego landshafta sovremennymi metodami [Experience of documenting Shulgan-Tash (Kapovaya) Cave and the surrounding landscape by modern methods]: Kratkiye Soobscheniya Instituta Arkeaologii [Brief Communications from the Institute of Archeology], v. 261, p. 67–81, https://doi.org/10.25681/IARAS.0130-2620.261.67-81.

Tizzard, A., and Horne, P., 2021, The disappearance of Slade Lake, Cumberland County, Nova Scotia, Canada: Atlantic Geology, v. 57, p. 133–134, https://www.erudit.org/en/journals/ageo/2021-v57-ageo05855/1076521ar.pdf.

Tkachev, S.A., 1999, Peshchera Ozhiganova: Nachalo gidrospeleosistemy Peshchery Shulgan-Tash: Izucheniye prirody v zapovednikakh Bashkortostana. [Ozhiganova Cave: The Beginning of the Shulgan-Tash Cave hydrosystem: Nature Studies in the Reserves of Bashkortostan, Miass, Chelyabinsk Oblast, Russia, Geotour, v. 1, p. 104–111.

Tsyganov, A.N., Kupriyanov, D.A., Babeshko, K.V., Borisova, T.V., Chernyshov, V.A., Volkova, E.M., Chekova, D.A., Mazei, Y.A., and Novenko, E.Y., 2019, Autogenic and allogenic factors affecting development of a floating *Sphagnum*-dominated peat mat in a karst pond basin: The Holocene, v. 29, p. 120–129, https://doi.org/10.1177/0959683618804631.

Vakhrushev, G.V., 1960, Zagadki Kapovoy Peshchery (Shulgan) [Mysteries of the Kapovaya Cave (Shulgan)], Ufa, Bashkortostan Republic, Russia, Akademiya Nauk CCCP, 32 p.

Volkova, E.M., 2010, The way of floating peat formation in karst depressions of European Russia: Open Geography Journal, v. 3, p. 67–72, https://doi.org/10.2174/1874923201003010067.

White, W.B., 1988, Geomorphology and Hydrology of Karst Terrains, New York, Oxford University Press, https://archive.org/details/geomorphologyhyd0000unse.

GUIDE TO AUTHORS

The *Journal of Cave and Karst Studies* is a multidisciplinary journal devoted to cave and karst research. The Journal is seeking original, unpublished manuscripts concerning the scientific study of caves or other karst features. Authors do not need to be members of the National Speleological Society, but preference is given to manuscripts of importance to North American speleology.

LANGUAGES: The *Journal of Cave and Karst Studies* uses American-style English as its standard language and spelling style. A second abstract in another language will be considered when room allows and is determined necessary. In the case of proper names, the *Journal* tries to accommodate other spellings and punctuation styles. In cases where the Editor-in-Chief finds it appropriate to use non-English words outside of proper names (generally where no equivalent English word exist), the *Journal* italicizes them. Common abbreviations, i.e., e.g., et al., etc. should appear in normal text. Authors are encouraged to write for our combined professional and amateur readerships. Spell out first use of acronyms.

CONTENT: Each paper will contain a title, the authors' names and addresses, an abstract, and the text of the paper, including a summary or conclusions section. Acknowledgments and references are to follow the text. Manuscripts should be limited to 6,000 words and no more than 10 figures and 5 tables. Larger manuscripts may be considered, but the Journal reserves the right to charge processing fees for larger submissions.

ABSTRACTS: An abstract stating the essential points and results is required. The abstract is to be a summary, not a promise of what topics are covered in the paper.

STYLE: The *Journal* consults The Chicago Manual of Style on most general style issues.

REFERENCES: References to previously published work should be followed by the relevant author's name and date in parentheses. All cited references are to be listed alphabetical at the end of the manuscript with senior author's last name first, followed by date of publication, title, publisher, volume, and page numbers. Geological Society of America format should be used (see http://www.geosociety.org/gsa/gsa/pubs/Ref-Guide-Examples). Please do not abbreviate periodical titles. Web references are acceptable when deemed appropriate. The references should follow the style of: Author (or publisher), year, Webpage title: Publisher (if a specific author is available), full URL (e.g., http://www.usgs. gov/citguide.html), and the date the website was accessed in brackets. If there are specific authors given, use their name and list the responsible organization as publisher. Citations within the text should read: (Author, Year).

SUBMISSION: Manuscripts are to be submitted via the PeerTrack submission system at https://www.editorialmanager.com/jcks. Additional instructions are provided at that address. You will be prompted to establish a login and password, after which you will enter information about your manuscript and upload your manuscript, tables, and figure files. Manuscript files can be uploaded as DOC, WPD, RTF, TXT, or LaTeX. Note: LaTeX files should not use any unusual style files; a LaTeX template and BiBTeX file may be obtained from the Editor-in-Chief. Table files can be uploaded as DOC, WPD, RTF, TXT, XLS, or LaTeX files and figure files can be uploaded as TIFF, AI, EPS, or CDR files. The including of supplementary materials should be minimized. Supplemental data or other materials (e.g. video clips) may be placed on the Journal's website at the discretion of the Editor-in-Chief. The data used within a paper must be made available upon request during the review process.

FIGURES: Figures and lettering must be neat and legible. A list of figures and their captions should be provided at the end of the text or as a separate document and not within the figure. Figures should be numbered in sequence and referred to in the text by inserting (Fig. x). Most figures will be reduced; hence, the lettering should be large. Photographs must be sharp and high contrast. Figures must have a minimum resolution of 300 dpi for acceptance. Please minimize the use of JPEG images.

TABLES: See https://caves.org/wp-content/uploads/2022/01/JCKS_Tables.pdf. for table layout guidelines.

MEASUREMENTS: All measurements will be in the International System of Units (SI or metric) except when quoting historical references. Other units will be allowed where necessary if placed in parentheses following the SI units.

DISCUSSIONS: Critical discussions of papers previously published in the Journal are welcome. Authors will be given an opportunity to reply. Discussions and replies must be limited to a maximum of 1000 words and discussions will be subject to review before publication. Discussions must be within 12 months after the original article appears.

COPYRIGHT AND AUTHOR'S RESPONSIBILITIES: The submitted work should represent original work of the author(s) that has not been previously published. It is the author's responsibility to clear any copyright or acknowledgement matters concerning text, tables, or figures used from others. Authors should address sensitive or legal issues such as landowner and land manager concerns or policies, verify that the work was conducted using necessary permissions and permits, and minimize the disclosure of sensitive features and cave locations.

PROCESS: Submitted manuscripts are assigned to the appropriate Associate Editor and sent out to at least two experts in the field for review. Reviewed manuscripts are then returned to the author for consideration of the referees' remarks and revision, where appropriate. Revised manuscripts are returned to the Associate Editor who then recommends acceptance or rejection. The Editor-in-Chief makes final decisions regarding publication. Upon acceptance, the senior author will be sent one set of PDF proofs for review prior to publication.

Journal of Cave and Karst Studies

Volume 87 Number 1 March 2025

CONTENTS